EFFECTS ON PORE PRESSURE, CONFINING PRESSURE AND PARTIAL SATURATION ON PERMEABILITY OF SANDSTONES

A DISSERTATION
SUBMITTED TO THE DEPARTMENT OF GEOPHYSICS
AND THE COMMITTEE ON GRADUATE STUDIES
OF STANFORD UNIVERSITY
IN PARTIAL FULFILLMENT OF THE REQUIREMENTS
FOR THE DEGREE OF
DOCTOR OF PHILOSOPHY

By
Joel D. Walls

October 1982

TABLE OF CONTENTS

TABLE OF CONTENTS (Continued)

EFFECTS OF PORE PRESSURE, CONFINING PRESSURE AND PARTIAL SATURATION ON PERMEABILITY OF SANDSTONES

ABSTRACT

Permeability to distilled water and brine has been measured on a suite of sandstone cores with a range of clay contents. Pore pressure and confining pressure were varied systematically in order to determine their relative effects. It was observed that in the low or no clay samples, pore pressure and confining pressure had equal magnitude effects on liquid permeability. However, in the samples with significant clay content, pore pressure had a larger magnitude effect on permeability than confining pressure. This is consistent with the idea of clays being a more compressible phase in the pore space with the sandstone framework being more rigid.

On a suite of tight gas sand samples, the effects of confining pressure and partial water saturation were measured using a pulse decay permeameter. The "infinite reservoir" technique was used with an analytical solution to the diffusion problem which allows accurate determination of gas permeability from a transient pulse decay. It was observed that confining pressure from near zero to in situ lithostatic levels can have a large effect on permeability in these samples. Reduction of gas permeability by a factor of 6 to 10 was common. Partial water saturation can have a much larger effect, however. In going from dry to 50% of the pore space water saturated, some samples' gas permeabilities dropped by a factor of 100. Most of these

phenomena can be attributed to the crack-like pore space in tight gas sands, with clay content being of secondary importance.

The pulse-decay permeameter was refined by adding multi-sample capability and computer control. Using this fully automated system, the effects of different brine solutions on gas permeability was measured. Results of this experiment show that type and amount of dissolved salts has little effect on the shape of the gas permeability vs. water saturation curve, again indicating that the clays present in those samples are not having a strong affect on gas flow behavior.

CHAPTER 1

PORE PRESSURE AND CONFINING PRESSURE: EFFECTS ON HIGH PERMEABILITY SAMPLES

ABSTRACT

Permeability of seven sandstone samples was measured in the laboratory with distilled water as the pore fluid. Pore pressure was varied between 20 and 300 bars and confining pressure between 50 and 600 bars. All experiments were at room temperature. Confining pressure, P_c, and pore pressure, P_p, were varied independently to determine their effect on absolute permeability. In sandstones with larger amounts of clay the change in permeability, k, due to pore pressure $\beta = \partial k/\partial P_p$ was greater than due to confining pressure $\alpha = \partial k/\partial P_c$. The ratio of β/α for a clean St. Peter sandstone was close to 1, indicating that permeability was essentially obeying the common effective stress law $\overline{P} = P_c - P_p$. On the other extreme, a sample of Bandera sandstone with about 20% clay had a β/α value of 7.1. This implies that pore pressure is seven times more effective in changing permeability than confining pressure. Other samples with intermediate clay contents had β/α values ranging from 0.5 md for high clay content to 950 md in clay free rocks. We conclude that for constant porosity in the rock studies, the permeability decreases and the ratio β/α increases systematically with clay content. The results are valid over a range of 1000 in permeability and a factor 10 β/α.

INTRODUCTION

The purpose of this experiment was to determine how variation of confining pressure (P_c) and pore pressure (P_p) effects the absolute hydraulic permeability in shaley sandstones. It is often assumed that permeability (k) of rocks is changed only by the effective stress ($P_c - P_p$) but recent experiments (Zoback, 1975) have indicated that pore pressure may have a greater effect on permeability than confining pressure in some rocks. To investigate this phenomenon a system for measuring permeability under conditions of variable pore pressure and confining pressure was constructed. Six samples were chosen to prepresent a variety of sandstone types. Measurements were made at room temperature (20°C ± 0.5°) using distilled water as the pore fluid.

EXPERIMENTAL DESIGN

A schematic diagram of the experimental system is shown in Figure 1.1. The sample, in the form of a right circular cylinder, is held between two stainless steel end pieces with 2 layers of screen wire separating sample and end piece. This is to insure even distribution of pore fluid across the end of the sample. The sample is jacketed with Tygon tubing and placed in a pressure vessel. Two tubes on each end of the sample extend through the top of the pressure vessel and connect to the pore pressure system. This system consists of a positive displacement variable speed pump, a differential pressure transducer, an air driven fluid pump to apply pore pressure and a Heise gauge to measure the pore pressure. Permeability is given by Darcy's Law

$$K = \frac{a\mu L}{A\Delta P} \tag{1.1}$$

where k = permeability in darcy

q = flow rate in cm^3/sec

μ = fluid viscosity in centipoise

L = sample length in cm

A = sample cross-section in cm^2

ΔP = pressure differential across sample in bars.

The sandstone samples chosen were Bandera, Berea, Massilon, Brownstone, and St. Peter. These samples represent a wide variety of permeabilities and compositions whereas they all have quite similar porosities around 20%. Most notable is the range of clay content, which is zero for the St. Peter to 21% for the Bandera (Table 1.1). In addition to the sandstone a sample of fused

aluminum oxide was included which is totally inert with respect to water and can be used as a permanent standard for the system.

The samples were prepared by first coring from larger blocks and then cutting to length. The length and diameter were then measured to 0.10 mm and then the sample was weighed, first dry and then saturated to determine connected porosity. The samples were stored in a desiccator until time for measurement when they were resaturated with distilled water and then mounted in the pressure vessel. An initial confining pressure of 40 bars and pore pressure of 20 bars was applied and the sample was left overnight to insure complete saturation. The circulating pump was then started and permeability was measured continuously for about 10 - 20 minutes or until a stable value of permeability was reached. In some samples an initial decrease in permeability of up to 10% occurred in the first 1 - 5 minutes of pumping. After permeability reached a constant value then confining pressure and pore pressure were varied systematically as described below.

In order to determine the effect of confining pressure on permeability the pore pressure was held at a constant value to 20 bars while the confining pressure was increased in 50 or 100 bar steps up to a maximum P_c between 500 and 1000 bars depending on the sample. At each point the permeability was measured at least three times and an average value of k was calculated. Permeability was also measured as P_c was decreased back to its original values. This procedure was then repeated. On the first cycle most samples showed some permanent loss of permeability, usually about 5 to 10%. On the second cycle no observable permanent change occurred and those values of permeability are reported here.

To determine the effect of pore pressure on permeability the effective stress ($P_c - P_p$) was held at 50 bars while pore pressure was increased from 20 bars up to a maximum of 300 bars. P_p was then reduced in 20 bar steps back to its original value. The permeability was calculated from the average of at least three measurements at each value of P_p.

To compare the effect of P_c and P_p on the permeability of the different samples, permeability was normalized by dividing by k_o, the permeability k at $P_c = P_p = 0$. Figure 1.2 shows normalized permeability (k/k_o) as a function of confining pressure with constant pore pressure at 20 bars for the six samples studied. The straight lines throughout the data are determined by least square fitting. Figure 1.3 shows normalized permeability vs. pore pressure with constant ($P_c - P_p$) = 50 bars for all samples.

DATA ANALYSIS

The data for each sample shown in Figures 1.2 and 1.3 may be described by an approximate relationship of the form

$$k = k_0 - aP_c + bP_p \quad . \tag{1.2}$$

Normalizing the expression yields

$$k/k_0 = 1 - \alpha P_c + \beta P_p = 1 - \alpha(P_c - \frac{\beta}{\alpha} P_p) \quad , \tag{1.3}$$

where $\alpha = a/k_o$ and $\beta = b/k_o$. Letting $k/k_o = \bar{k}$ and $\Delta P = P_c - P_p$ we obtain

$$\left.\frac{d\bar{K}}{dP_c}\right|_{P_p} = \left.\frac{d\bar{K}}{d(\Delta P)}\right|_{P_p} = -\alpha \tag{1.4}$$

$$\left.\frac{d\bar{K}}{dP_p}\right|_{P_c} = \beta \tag{1.5}$$

and

$$\left.\frac{d\bar{K}}{dP_p}\right|_{\Delta P} = \beta - \alpha = -a(1 - \frac{\beta}{\alpha}) \quad . \tag{1.6}$$

The effect of confining pressure on permeability with constant pore pressure is given by α. The effect of pore pressure on permeability with constant confining pressure is given by β and the effect of pore pressure on

permeability with constant effective stress ($P_c - P_p$) is given by $\beta - \alpha$. The slopes of the lines in Figure 1.2 give α for each sample and the slopes of the lines in Figure 1.3 give ($\beta - \alpha$) for each sample. The quantity β/α is thus a good indicator of the effect of pore pressure relative to confining pressure: When $\beta/\alpha < 1$ then P_p is <u>less</u> effective than P_c in changing permeability; when $\beta/\alpha = 1$ then P_c and P_p have <u>equal</u> effects on permeability; and when $\beta/\alpha > 1$ P_p is <u>more</u> effective than P_c in changing permeability.

Table 1.2 shows the values of k_o, $\beta - \alpha$, α, β/α, porosity and clay content for the five sandstones and for aluminum oxide. For the case of AL_2O_3 β/α is less than 1 which means confining pressure is having larger effect on permeability than pore pressure. This can be explained on the basis of pore volume reduction. Nur and Byerlee (1971) have shown that confining pressure can have a larger effect on pore volume changes than pore pressure in a granular material if the compressibility of the individual grains is less than the compressibility of the sample as a whole. This is the case for the fused aluminum oxide.

For the St. Peter sandstone which is 99 to 100% quartz, β/α is nearly equal to 1. This implies that the material is obeying an effective stress law for permeability which is what we would expect for a porous elastic solid with a bulk compressibility much greater than grain compressibility. Note here the absence of significant clay content for the St. Peter. The Brownstone sample has not yet been analyzed for clay content but it is clear from its β/α value of 2.4 that pore pressure is effecting its permeability considerably more than confining pressure. Massilon sandstone with approximately 5 - 6% kaolinite in the pores shows an even larger β/α of 3.2. Berea sandstone with 8% kaolinite has a much lower k_o than the above samples and its β/α of 3.3 Bandera sandstone has the lowest initial permeability and

the largest kaolinite content and also by far the largest $\beta/\alpha = 7.1$. Consequently we can discern a clear trend of larger β/α in rocks with higher clay content (Figure 1.4). For comparison, two samples are shown which were measured by Zoback (1975). Berea and Massilon sandstone using Shell Tellus oil which is considered inert in contact with clay and other minerals found in sandstone. The values of k_o, β/α, porosity and clay content as measured by Zoback are all very similar to the values measured in this experiment on the same rock types. Zoback's data also shows the sample with larger clay content having a larger value of β/α.

If β/α is in some way related to clay content as is suggested by the data the obvious question is why? In general it can be said that confining pressure can change permeability only to the extent that it can deform the rock skeleton. Pore pressure in contrast can act directly on the pore space, including clay minerals. A conceptual model was proposed by Zoback where a porous solid with clay is approximated by a hollow cylinder with high compressibility surrounded by another cylinder with low compressibility. If external pressure is changed the internal dimensions and hence permeability will be little affected. If the internal pressure is changed the soft lining will compress and could produce a significant change in internal dimensions and hence in permeability. The major objection to such a model is that it is doubtful if clay can be treated as an impermeable yet highly compressible material which deforms when pore pressure is applied. However, not all the conditions and parameters which affect clay swelling are fully understood. Conceivably changes in fluid pressure might cause changes in clay particle packing and hence changes in permeability.

Finally the results show that not just the rate of change but permeability itself is strongly correlated with clay content. Figure 1.5 shows the empirical relation we found between permeability and clay content for our samples - which have similar porosities. Thus the permeability of Berea sandstone, with 20% porosity and 8% clays, is 20 times smaller than St. Peter sandstone, also with 20% porosity, but without clay. The total range of sandstone porosities in our samples is about 6%, whereas permeability changes by three orders of magnitude. A clear conclusion from these data is that no simple relation between porosity and hydraulic permeability exists in shalely sandstone.

SUMMARY

It was found that for a clean consolidated sandstone, pore pressure and confining pressure have roughly equal effects on permeability, but sandstones with significant fractions of clay are more sensitive to changes in pore pressure. The effect may be very pronounced in high clay content samples with achange in P_p producing almost an order of magnitude larger effect on permeability than an equivalent change in confining pressure. It was also observed that the effect is present whether the pore fluid is an inert oil or distilled water.

Furthermore, permeability varies by three orders of magnitude from 1 to 5×10^{-4} darcy with clay content from 1% to 20% for shalely sandstones all with the same porosity.

The results may suggest that the permeability in tight shalely rocks in general is increasingly more sensitive to pore pressure with increasing shaliness, so that flow rates in rocks such as the devonian shales may be very much affected by borehole pressures.

REFERENCES

1 Nur, A., and J. D. Byerlee, 1971, "An Exact Effective Stress Law for Elastic Deformation of Rocks with Fluids," J. Geophys. Res., Vol. 76, 6414-6419.

2 Zoback, Mark D., 1975, "High Pressure Deformation and Fluid Flow in Sandstone, Granite and Granular Materials," Ph.D. Thesis, Dept. of Geophysics, Stanford University.

TABLE 1.1 PERMEABILITY EXPERIMENT SPECIFICATIONS

Range of Permeability: 1.0 md to 2000 md

Accuracy: ± 2%

Resolution: ± 0.5%

Confining Pressure: 10 to 2000 bars

Pore Pressure: 5 to 300 bars

Temperature: Ambient

Pore Pressure Gradient: < 1 bar/cm

Pore Fluid Flow Rate: 0 to 2 liter/hr.

Sample Size: 1 inch diameter x 3.5 cm long (typ.)

TABLE 1.2 SAMPLE CHARACTERISTICS

Sandstone	ϕ	Mineralogy
Bandera	17%	56% quartz, 10-25% calcite, 21% Kaolinite
Berea	20%	70-80% quartz, 2-9% calcite, 5% feldspar, 8% kaolinite
Massilon	23%	94% quartz, 6% clay
St. Peter	20%	99% quartz
Fused Al_2O_3	26%	99% Al_2O_3

TABLE 1.3 PERMEABILITY AND PRESSURE SENSITIVITY OF SAMPLE SUITE

	Ko (md)	$\beta - \alpha$ $(bar^{-1})x10^{-4}$	$-\alpha$ $(bar^{-1})x10^{-4}$	(β/α)	ϕ (%)	Clay Content %	Pore Fluid
Al_2O_3	817	-.82	-1.43	0.43	26	0	Distilled water
St. Peter	944	.12	- .84	1.2	20	<1%	"
Brownstone	624	2.5	-1.8	2.4	21		"
Massillon	737	3.14	-1.4	3.2	23	5-6%	"
Berea	52	7.8	-3.3	3.3	20	8%	"
Bandera	0.4	33.	-5.4	7.1	16	20%	"
Berea (Zpback, '75)	42	10.	-3.4	4.0	19	8%	Shell Tellus Oil #15
Massillon (Zoback, '75)	995	5.9	-2.3	3.5	24	6%	"

$$\alpha = \frac{\partial K}{\partial P_c}\Big|_{P_p} \qquad \beta = \frac{\partial K}{\partial P_p}\Big|_{P_c}$$

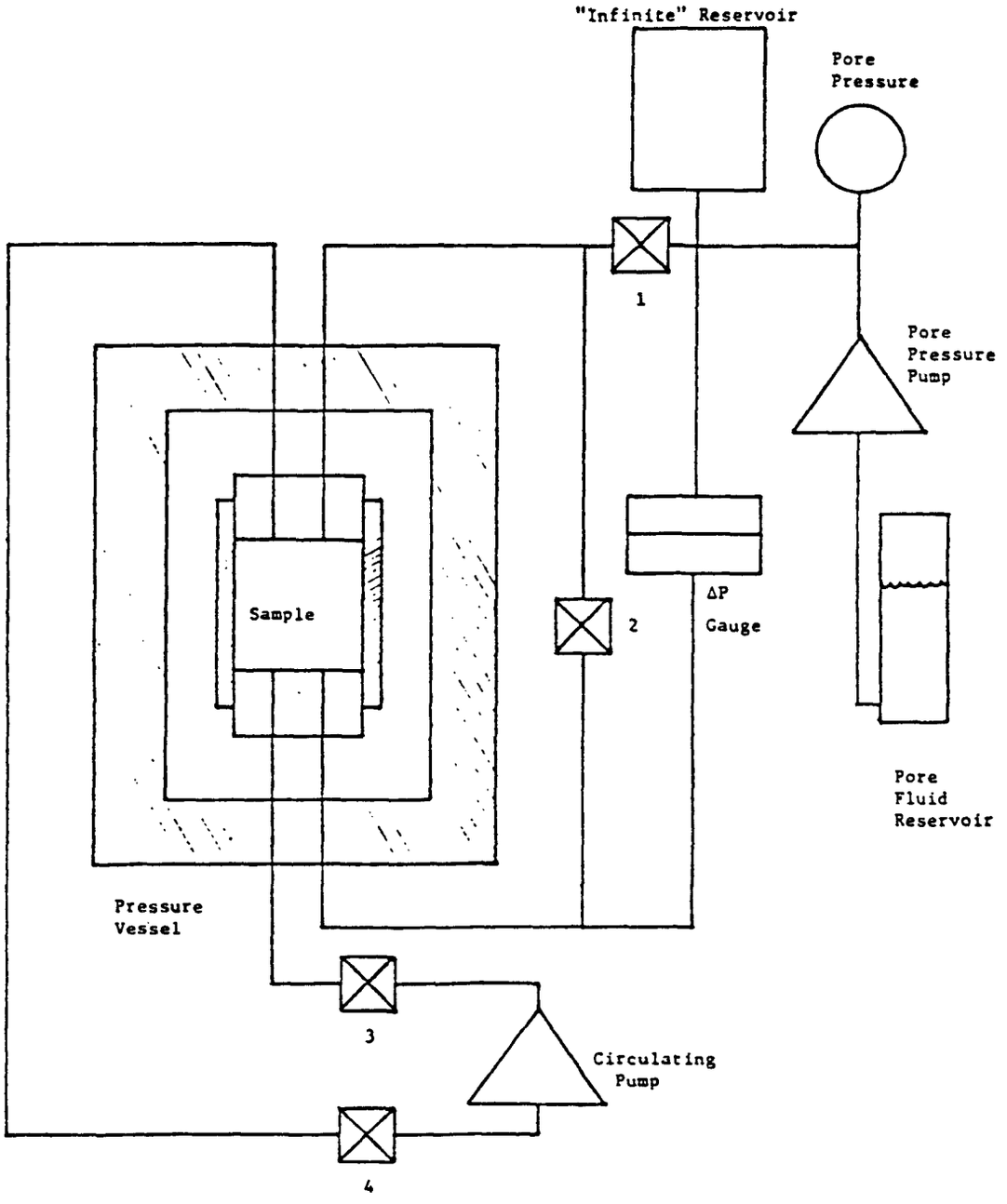

FIGURE 1.1 Schematic presentation of permeability system with independently controlled confining and pore fluid pressure.

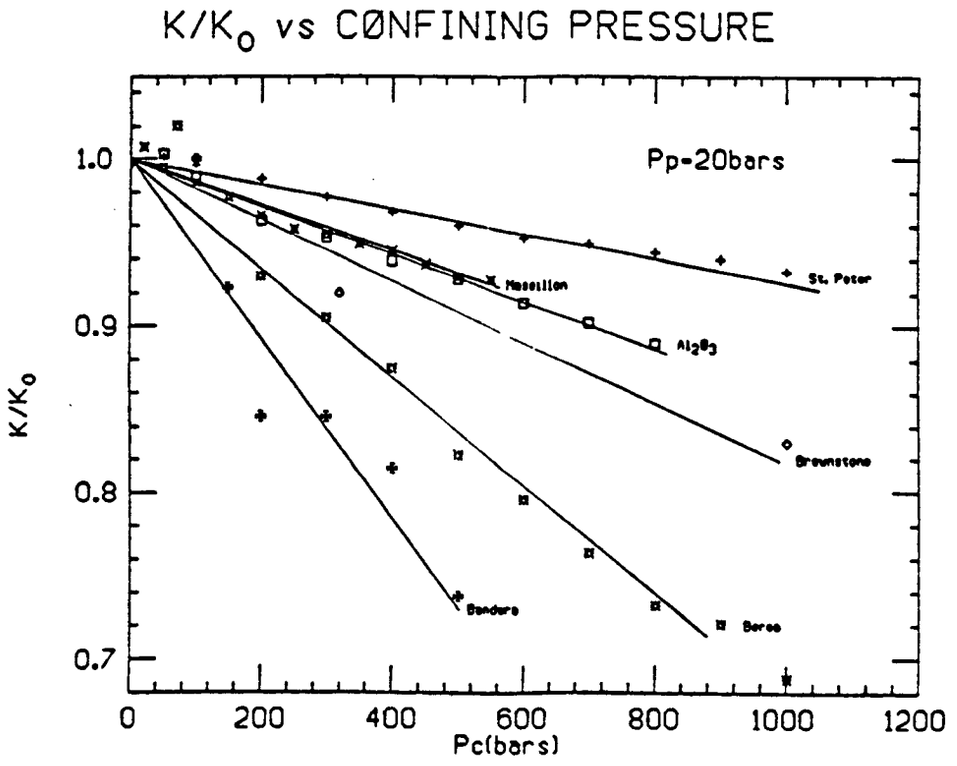

FIGURE 1.2 Effect of confining pressure on water permeability with constant pore pressure.

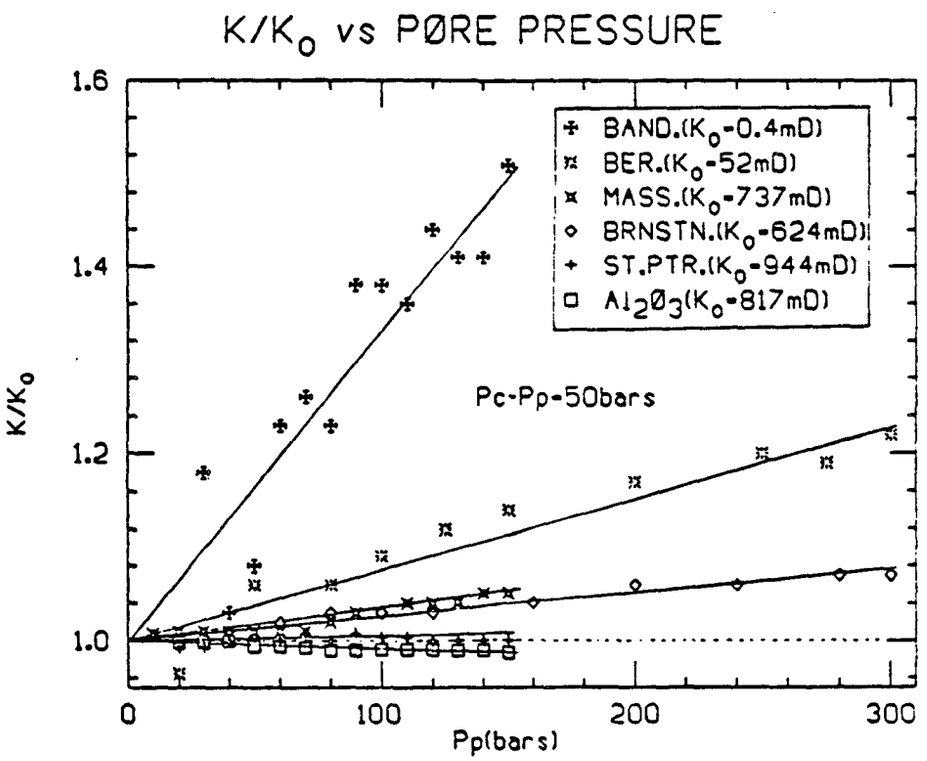

FIGURE 1.3 Effect of pore pressure on water permeability with constant effective pressure.

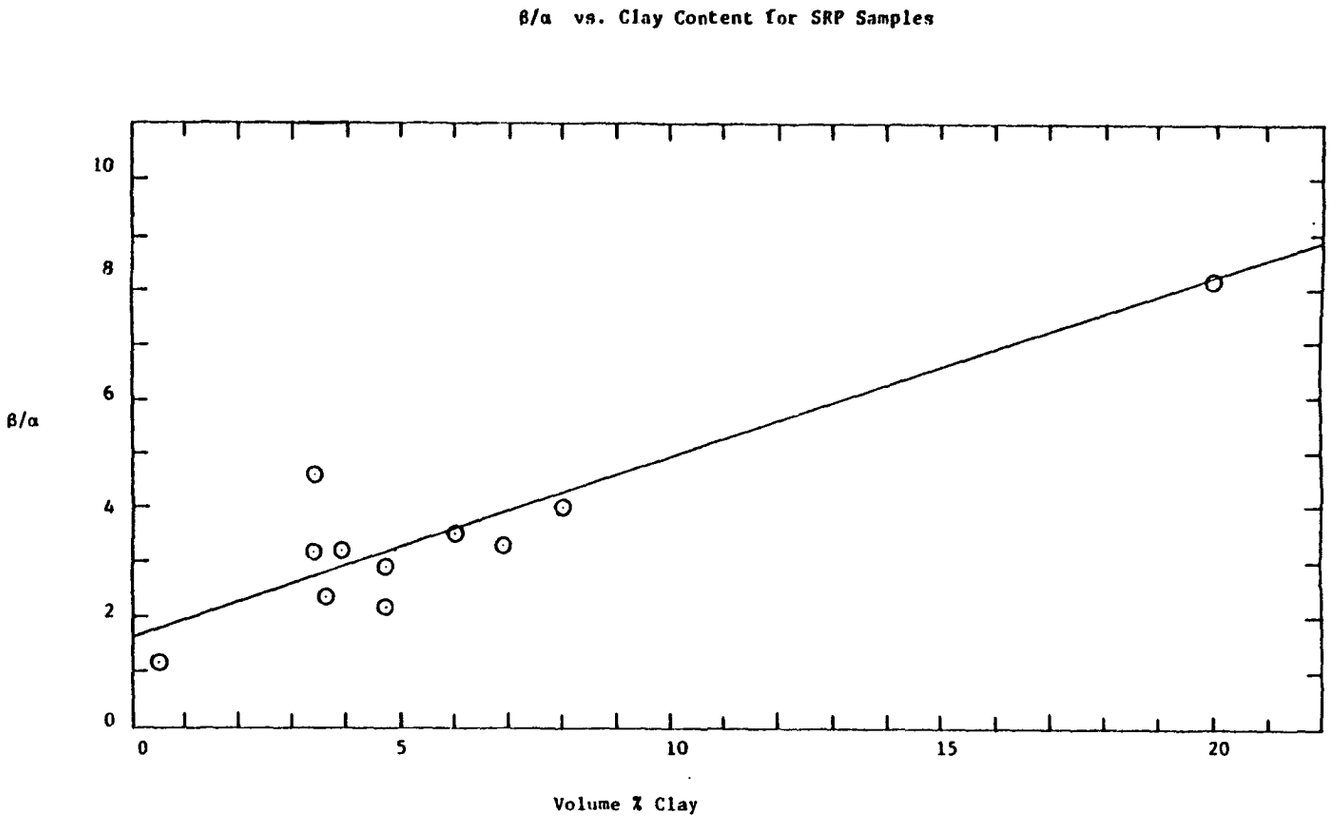

FIGURE 1.4 The dependence of the ratio β/α on the clay content in shaley sandstones. The ratio is defined as

$$\left[\partial\bar{K}/\partial\Delta P \,\middle|_{P_p} \Big/ \partial\bar{K}/\partial P_p \,\middle|_{\Delta P}\right] .$$

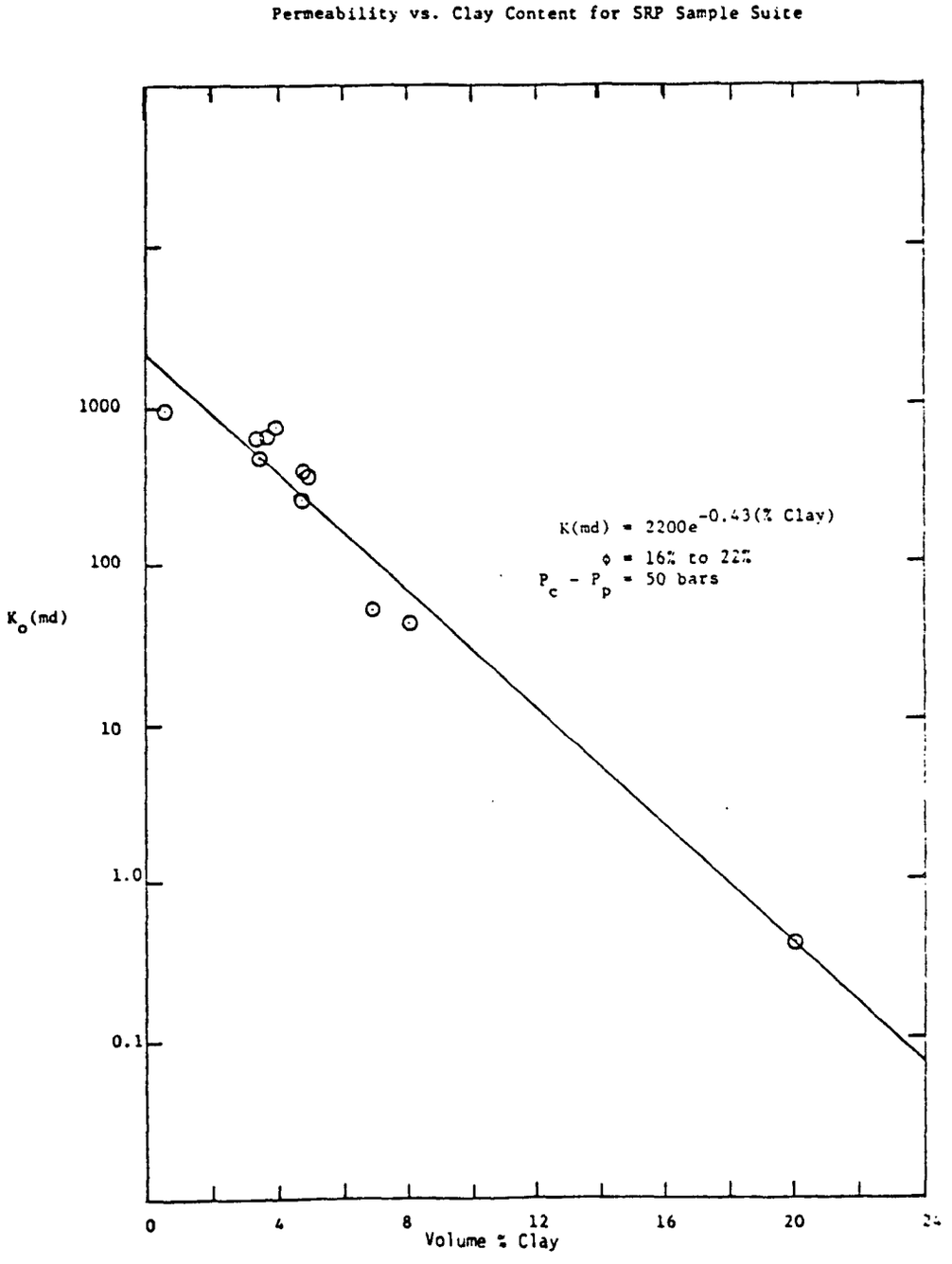

FIGURE 1.5 The dependence of hydraulic permeability on clay content in shaley sandstones.

CHAPTER 2

PULSE DECAY PERMEABILITY:

ANALYTICAL SOLUTION AND EXPERIMENTAL TEST

ABSTRACT

A new analytical solution is presented for the laboratory pulse decay permeability problem. Using this solution, permeability of a core sample can be calculated from the decay rate of a pressure pulse applied to one end of the sample. This development permits rapid, accurate measurement of permeability in samples such as tight gas sands, limestones and shales.

INTRODUCTION

Because of its usefulness in measuring very low permeability, the pulse decay technique has been often discussed in the literature. In this technique, a small pore pressure pulse is applied to one end of a jacketed sample and the pressure vs. time behavior is observed as the pore fluid moves through the sample from one reservoir to another. Brace, et al., (1968) gave an approximate solution to this problem with the assumption of a linear pressure gradient at all times. This simplification leads to a predicted exponential pressure vs. time decay. By means of numerical solutions Lin (1977) and Yamada and Jones (1979) have shown that the Brace solution can lead to significant errors in calculating permeability. These numerical solutions, however, are inconvenient to use and require considerable computer programming time. We will present an analytical solution based on realistic assumptions and boundary conditions.

EXPERIMENTAL TECHNIQUE

To better understand the theoretical problem a short description of the experiment is desirable. Figure 2.1 is a schematic of the system. Initially both valves are open and pressure is constant throughout the system. Next, valve 1 is closed and the pressure is changed slightly in the large Reservoir 1. Valve 1 remains closed for a few minutes to allow thermal effects to diminish (particularly important if the pore fluid is gas). Valve 2 is then closed and at time equal zero, valve 1 is opened. A small differential pressure between the reservoirs will be indicated by the ΔP transducer and will decrease with time. Pressure in Reservoir 1 remains constant during the decay. After the differential pressure has decreased by approximately 20% the decay is terminated by opening valve 2. This accelerates the equilibration of pressure so the next measurement can be made.

THEORY

As stated earlier, the pressure in Reservoir 1 remains essentially constant during the decay ($t \geq 0$) because the volume of Reservoir 1 (V_1) is much greater than the pore volume (V_p) or the volume of Reservoir 2 (V_2). It can be assumed that fluid viscosity (μ) is independent of position (x) in the sample and that fluid density (ρ), permeability (k) and porosity (ϕ) are only dependent on fluid pressure (P). By combining Darcy's law with the one-dimensional diffusion equation we obtain

$$(\beta_k + \beta)\left(\frac{\partial P}{\partial x}\right)^2 + \frac{\partial^2 P}{\partial x^2} = \frac{\mu\phi(\beta_s + \beta)}{k}\frac{\partial P}{\partial t} \tag{2.1}$$

where β is fluid compressibility, β_s is rock compressibility, and β_k is the dependence of permeability on pore pressure. The magnitude of the non-linear terms with respect to the linear ones is equal to $(\beta_k + \beta)P^o$, where P^o is the pressure pulse amplitude. Since $(\beta_k + \beta) \simeq 10^{-2}$ bar^{-1} (ref. 8) and $P^o \simeq 1$ bar, the product is small and hence non-linear terms can be ignored. If we further assume that $\beta_s \ll \beta$ then the equation of flow is

$$\frac{\partial^2 P}{\partial x^2} = \frac{1}{c}\frac{\partial P}{\partial t} \tag{2.2}$$

where $c = k/\mu\beta\phi$. The system can now be described by (2.2) and the following boundary and initial conditions:

$$\begin{aligned} &\text{Initial condition:} && P(x,t=0) = P_2^o \\ &\text{Boundary condition 1:} && P(x=0,t) = P_1 \\ &\text{Boundary condition 2:} && \frac{dP(x=L,t)}{dt} = -\kappa \left.\frac{\partial P}{\partial x}\right|_{x=L} \end{aligned} \tag{2.3}$$

where $\kappa = kA/\mu\beta V_2$. Boundary condition 2 results from fluid mass balance considerations at $x = 1$ and in volume V_2.

After the change of variable, $v(x,t) = P(x,t) - P_1$, we take the Laplace transform of the system. After developing and keeping the first terms we obtain

$$\overline{V} = \frac{P^o}{p} - \frac{P^o}{p} e^{-qx} + \frac{P^o}{p} \frac{cq + \kappa}{cq + \kappa} (e^{-q(2L-x)} - e^{-q(2L+x)}) \tag{2.4}$$

where $q^2 = P/c$ and p is the Laplace variable. This approximation is good for values of time such that

$$t \leq \frac{L^2}{c} \tag{2.5}$$

(Carslaw and Jaeger, 1959; Goldstein, 1932). This time allows the pressure pulse to decay to about one-half of its initial value regardless of the permeability and since we need only about a 20% decrease to obtain sufficient data, this time limit does not affect measurement accuracy.

Using inverse Laplace transforms, it can be shown that the solution to (2.4) is

$$P_1 - P_p(x,t) = (P_1 - P_2^o) \left[1 - \operatorname{erfc} \frac{x}{2\sqrt{ct}} - \operatorname{erfc} \frac{2L - x}{2\sqrt{ct}} + \operatorname{erfc} \frac{2L + x}{2\sqrt{ct}} \right.$$

$$+ 2e^{\kappa/c(2L-x) + \kappa^2 t/c} \cdot \operatorname{erfc}\left(\frac{2L - x}{2\sqrt{ct}}\right) + \kappa\sqrt{t/c}$$

$$\left. - 2e^{\kappa/c(2L+x) + \kappa^2 t/c} \cdot \operatorname{erfc}\left(\frac{2L + x}{2\sqrt{ct}} + \kappa\sqrt{t/c}\right) \right] \tag{2.6}$$

where

$$\text{erfc } x = 1 - \frac{2}{\sqrt{\pi}} \int_0^x e^{-t^2}\, dt,\ c = \frac{k}{\mu\beta\phi} \text{ and } \kappa = \frac{A}{\beta\mu V_2} \quad .$$

DISCUSSION

To see if (2.6) actually describes the pressure vs. time behavior in our system we carefully determined the values of all the variables in (2.6). The sample used was a Spirit River tight sandstone core 5.08 cm in diameter and 6.7 cm long. The pore fluid was nitrogen at 140 bars pressure and 20.5°C. Reservoir and connecting line volumes were measured to within ±0.1%. The only remaining unknown was permeability itself and this was measured using an independent steady state technique similar to that used by Jones and Owens (1980). The pulse-decay test was then performed and the actual decay was compared to that predicted by (2.6). The experimental and predicted decay curves are shown in Figure 2.2. Similar tests have been performed on many types of samples always with the result that experiment and theory closely agree. For comparison, we also show in Figure 2.2 the exponential decay curve as predicted by Brace, et al., (1968). The magnitude of the discrepancy between the exponential solution and ours depends upon several experimental parameters, especially the volume ratio V_p/V_2. In our case the error resulting from using the exponential solution is about 25% but it can be much larger. A solution very similar to ours has recently been obtained, with slightly different boundary conditions, by Hsieh, et al., (1980).

Because (2.6) cannot be solved explicitly for k, we have devised a simple iterative computer program to find k from the experimental pulse decay. This program can be run on any desk top computer or programmable calculator. Permeabilities calculated from equation (2.6) are within ±5% of steady-state measurements over a wide range of permeability.

NOMENCLATURE

A = cross sectional area of sample

k = permeability

$c = k/\mu\beta\phi$

L = sample length

P = pore pressure

P_1 = pore pressure at $x = 0$

P_2 = pore pressure at $x = L$

P_2^o = pore pressure at $x = L$ and $t = 0$

$P^o = P_2^o - P_1$ = magnitude of pressure pulse

t = time

V_2 = volume of Reservoir 2

$v(x,t) = P(x,t) - P_1$

$\bar{v}$ = Laplace transform of v

x = position along sample

β = fluid compressibility

β_s = rock compessibility

$\beta_k = \frac{1}{k}\frac{dk}{dp}$

$\kappa = \frac{kA}{\mu\beta V_2}$

ϕ = sample porosity

ρ = fluid density

μ = fluid viscosity

REFERENCES

1 Brace, W.F., J.B., Walsh, and W.T. Frangos, 1968, Permeability of granite under high pressure, J. Geophys. Res., Vol. 73, p. 2225-2236.

2 Carslaw, H.S., and J.C. Jaeger, 1959, Conduction of Heat in Solids, 2nd ed., Oxford University Press, London, p. 510.

3 Goldstein, S., 1932, The application of Heavisides' operational method to the solution of a problem in heat conduction, Agnew. Math. Mech., Vol. 12, p. 234.

4 Hsieh, P.A., J.V. Tracy, C.E. Neuzil, J.D. Bredehoeft, and S.E. Silliman, A transient laboratory method for determining the hydraulic properties of "tight" rocks, submitted to International Jour. of Rock Mechanics.

5 Jones, F.O., and W.W. Owens, 1980, A laboratory study of low permeability gas sands, Jour. of Pet. Tech., Vol. 32.

6 Lin, W., 1977, Compressible fluid flow through rocks of variable permeability, Lawrence Livermore Laboratory, UCRL-52304, p. 15.

7 Walls, J.D., A.M. Nur, and T. Bourbie, 1980, Effects of pressure and partial water saturation on gas permeability in tight sands: experimental results, Jour. of Pet. Tech., Vol. 34, April 1982, p. 930-936.

8 Yamada, S.E., and A.H. Jones, 1979, A review of a pulse technique for permeability measurement, Terra Tek., Inc., Salt Lake City, Report TR 79-8.

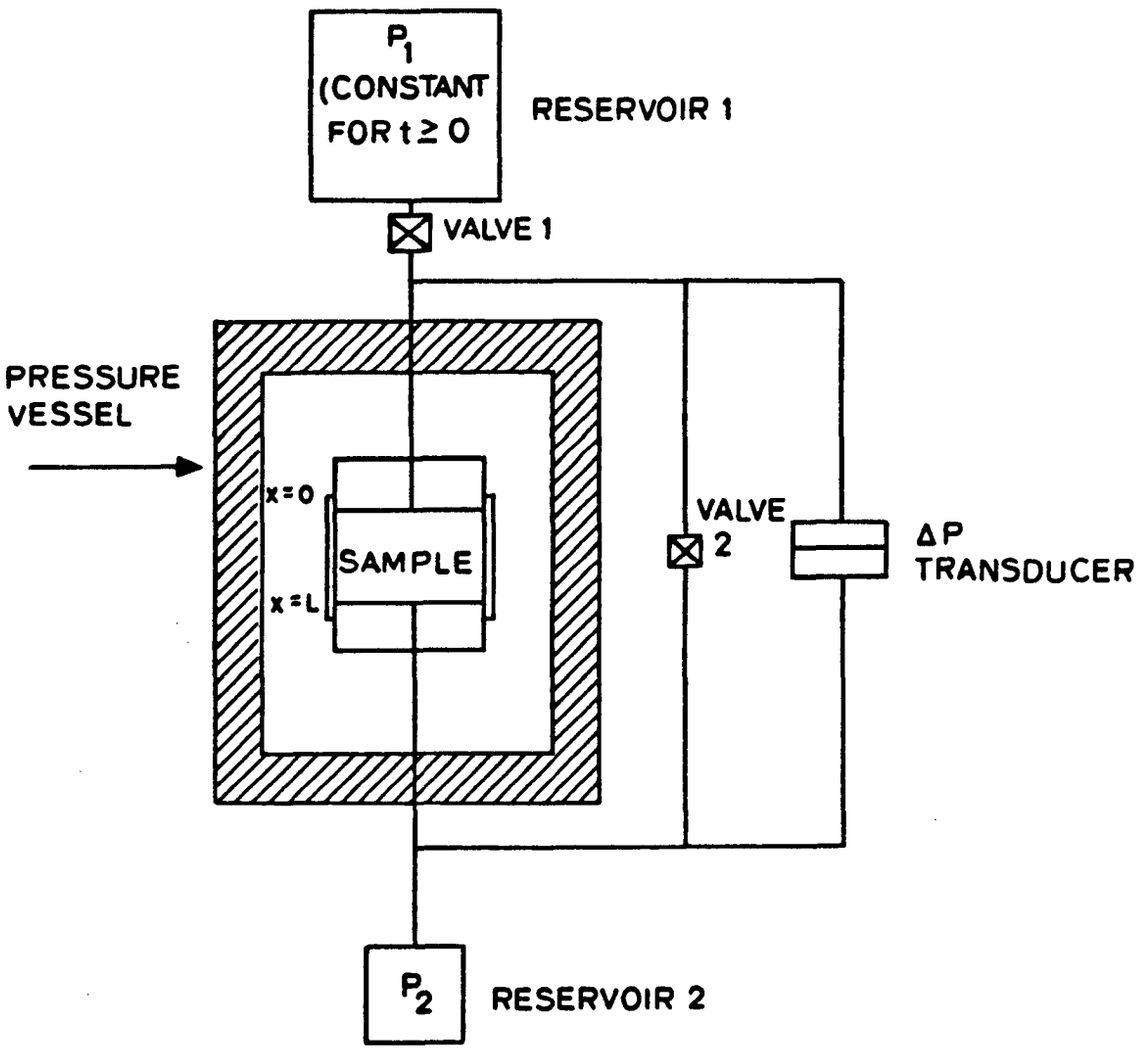

FIGURE 2.1 Schematic diagram of experimental system.

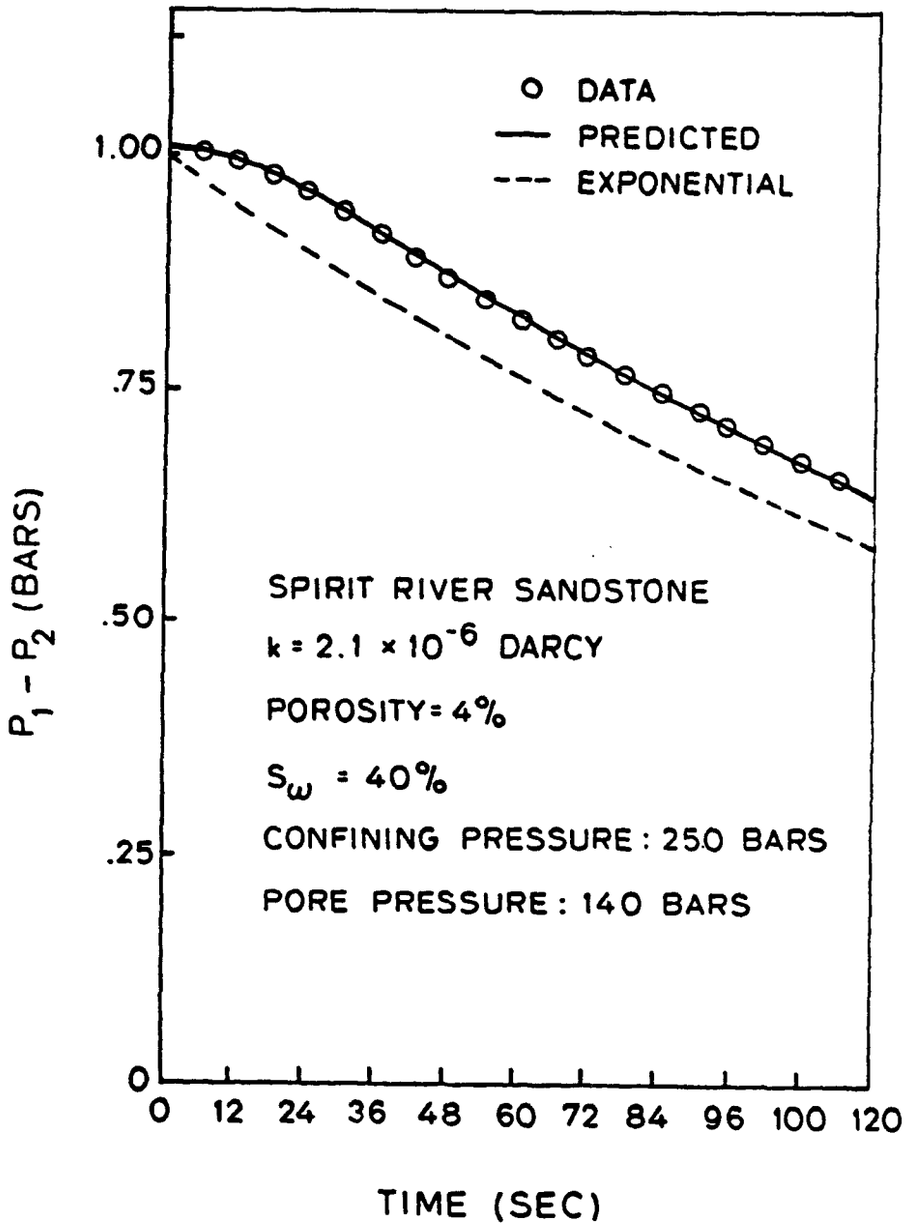

FIGURE 2.2 Theoretical and experimental pulse decay curves.

CHAPTER 3

EFFECTS OF PRESSURE AND PARTIAL WATER SATURATION ON LOW PERMEABILITY SAMPLES

ABSTRACT

Effective permeability to gas with various degrees of brine saturation has been measured in the laboratory for several very tight sandstones from the Spirit River formation of Alberta, Canada. Gas permeability as low as 20×10^{-9} darcy was measured successfully with a pulse-decay permeameter with nitrogen as the mobile fluid. Results show that gas permeability depends very strongly on the degree of saturation, with 40% saturation causing permeability to decrease an order of magnitude relative to the dry rock. Therefore, accurate knowledge of in-situ saturations is crucial before natural-gas production rates can be estimated in these formations. The experiments also show that confining pressure causes significant permeability reduction in these sandstones. A Spirit River sample recovered from 2133.6 m and subjected to in-situ levels of pore pressure and confining pressure shows a sevenfold reduction of gas permeability. It also was found that as brine saturation increased, the sensitivity of the rock's permeability to small changes in confining pressure increased.

INTRODUCTION

In recent years the importance of natural gas contained in low-permeability rock has increased tremendously. Reservoirs that once were dismissed as too tight now are being reevaluated in the light of new technology, such as massive hydraulic fracturing. In some cases, very tight gas-saturated rock is found directly above or below higher-permeability gas reservoirs, which creates the possibility that gas from the tight sand can migrate vertically into the producing formation. In any case, the permeability of the tight rock is of utmost importance in estimating the future recoverable reserves and the recovery rate.

The most common method of determining permeability in cores recovered from depth has been to measure air permeability in systems that apply only enough pressure to the core to prevent gas flow around the jacket. The results of this study indicate that gas permeability of tight sandstones determined by this method can be an order of magnitude higher than when in-situ levels of confining pressure are applied. Using steady-state flow methods to measure permeability of these samples with confining pressure becomes quite difficult because long times are required to establish equilibrium conditions. The addition of partial water or brine saturation further reduces gas permeability, compounding the problem. For these reasons, we have constructed an apparatus that uses a fast and accurate pulse-decay technique and allows independent control of confining pressure (P_c), pore pressure (P_p), and fluid saturation (S_w). Permeability as low as 20×10^{-9} darcy can be measured quite easily with this equipment.

The samples studied here are from the Spirit River member of the Fahler formation in western Alberta, Canada. This formation is believed to contain large volumes of natural gas in low-porosity, tight sandstones.[1] Spirit River samples are denoted by SR followed by a number that corresponds to the depth (in feet) from which they were recovered. Detailed mineralogy data from thin-sectioned, X-ray diffraction, and scanning electron microscope (SEM) methods are given in Table 3.1.

EXPERIMENTAL TECHNIQUE

A pulse-decay technique was used to make the large number of permeability measurements required for this experiment in a reasonable period of time. The concept of this method has been described by a number of experimenters, including Brace et. al.,[2] Sanyal et. al.,[3] and Zoback and Byerlee.[4] A schematic diagram of our apparatus is shown in Figure 3.1. The sample, a core 5.08 cm in diameter and 6 to 7 cm long, is held between two stainless-steel end caps and surrounded by a Teflon® jacket 0.4 cm thick. Two pieces of 100-mesh, stainless-steel screen wire separate the sample from each end cap to ensure even distribution of pore-fluid pressure across the sample ends. Each end cap has a pore-pressure tube leading to the outside of the hydrostatic confining-pressure vessel. The confining fluid is a mixture of ethylene glycol and water driven by an air-operated pump. The pore fluid is dry nitrogen that is brought to the desired pore pressure by a gas booster pump connected to a compressed-nitrogen bottle. After the sample is mounted and the desired pore pressure and confining pressure are applied, we allow several hours for pressure and temperature to reach equilibrium before any measurements are made.

Taking data with this system is quite simple. First, a 0.1-MPa pressure increase is applied to the pore-fluid reservoir (Reservoir 1) at one end of the sample, and to the differential-pressure transducer, whose output is recorded. As the nitrogen flows through the sample, the pressure in the downstream reservoir (Reservoir 2) begins to increase; as a result, the pressure differential (ΔP) between Reservoirs 1 and 2 begins to decrease toward zero with time. In practice, the pressure decay is terminated manually after it has decreased by 20 to 30%.

The curve for recorded differential pressure vs. time is used to calculate gas permeability using a highly accurate solution to the diffusion problem (discussed in the next section). After pore-pressure equilibrium is reestablished, a 0.1-MPa step decrease is applied and the decay time of P is measured again. Because the pore pressure used in this experiment is 14 to 15 MPa, the pulses are very small by comparison. The time required for each measurement ranges from about 2 minutes to more than 4 hour, depending on permeability. Klinkenberg corrections are unnecessary because of the high pore pressures and their small gradients. The equipment is surrounded by an insulated blanket, which reduces temperature fluctuation to less than 0.5°C.

SAMPLE PREPARATION

Sample saturation is achieved by 24-hour vacuum drying at 60 to 70°C followed by saturation with deaerated 1%-KCl brine at a pressure of 35 MPa. The fully saturated sample is removed 24 hours later and is weighed. Using the sample's dry weight and saturated weight, we determine the weight of pore water and, hence, pore volume. Because the sample is cut carefully to exact dimensions, we know its bulk volume precisely. Using the bulk volume and the pore volume determined from weighing, we can calculate porosity. To obtain a desired degree of partial saturation, the sample is dried gradually on a precise balance, which is used to infer the exact value of S_w. The sample is next installed in the pressure vessel; nitrogen flow is measured after allowing several hours for capillary forces to distribute the saturating fluid evenly. In this configuration, confining pressure (P_c) and pore pressure (P_p) are varied so that the dependence of permeability on P_c and P_p as a function of S_w is obtained. After the desired series of measurements is completed, the sample is removed and reweighed. In no case did the sample's water saturation change by more than 0.4%. The sample then is dried to a lower degree of saturation, and the process is repeated.

The saturation determined about is at zero confining pressure. To determine the degree of saturation at the P_c and P_p conditions in the pressure vessel, we measured the pore volume of the samples as a function of pressure in a separate experiment. Again following the saturation procedure described above, the Teflon-jacketed sample is placed in the pressure vessel and confining pressure is increased slowly. The total amount of water displaced at each step increase of P_c is measured with a calibrated pressure intensifier with resolution of about 0.1% of the sample's pore volume. The

results of a typical compressibility experiment are shown in Figure 3.2. This information, obtained for each sample, was used to calculate the actual saturation at experimental pressure conditions.

PULSE-DECAY SOLUTION

The pulse-decay permeability technique has been used by several investigators. Because the exact solution to the pulse-decay problem is complex, approximate solutions have been invoked. Brace et al., Sanyal et al., and Zoback and Byerlee ignored the nonlinear, transient pore pressure in the sample. A solution with unsteady flow was given by Miller;[5] however, the boundary conditions do not apply to the laboratory experiment. A numerical solution to the pulse-decay problem was given by Lin,[6] but with boundary conditions slightly different from our experiment. We have instead derived the analytical solution to the pulse-decay problem with any desired degree of accuracy. The solution predicts the shape of the decay curve accurately and gives permeability values that agree closely with those determined by a steady-state technique. The governing equation to be solved is the one-dimensional diffusion equation,

$$\partial^2 P_p / \partial x^2 = (1/c)(\partial P_p / \partial t) \quad , \tag{3.1}$$

where P_p is pore pressure, x is position along the sample, t is time, $c = k/\mu\beta\psi$ is hydraulic diffusivity, k is hydraulic permeability, β is fluid compressibility, μ is fluid viscosity, ψ is porosity.

Equation (3.1) must be solved subject to the initial condition of uniform pressure, $P_p(x,t=0) = P_2$, where P_2 is the pressure in volume V_2. The auxiliary conditions are that P_1, the pressure in volume V_1, remains constant during the decay and that at x=L, where L is the sample length, the mass flux balance leads to

$$dP_p \quad \frac{L,t}{dt} = -\kappa \left(\frac{\partial P_p}{\partial x} \right) x-L \quad , \tag{3.2}$$

where $\kappa = kA/\mu\beta V_2$, A is the sample's cross-sectional area, and V_2 is the downstream volume.

The solution is obtained by the Laplace transform method. It can be shown[7,8] that the exact solution for early time ($t<L^2/c$) is

$$P_1 - P_p(x,t) = (P_1 - P_2^o) \left[1 - \text{erfc} \frac{x}{2\sqrt{ct}} - \text{erfc} \frac{2L-x}{2\sqrt{ct}} + \frac{2L+x}{2\sqrt{ct}} \right.$$

$$+ 2e^{\kappa/c(2L-x) + \kappa^2 t/c} \cdot \text{erfc} \left(\frac{2L-x}{2\sqrt{ct}} \right) + \kappa\sqrt{t/c}$$

$$\left. - 2e^{\kappa/c(2L+x) + \kappa^2 t/c} \cdot \text{erfc} \left(\frac{2L+x}{2\sqrt{ct}} \right) + \kappa\sqrt{t/c} \right] \tag{3.3}$$

where

$$\text{erfc } x = 1 - \frac{2}{\sqrt{\pi}} \int_0^x e^{-t^2} dt, \; c = \frac{k}{\mu\beta\phi} \text{ and } \kappa = \frac{A}{\beta\mu V_2} \quad . \tag{3.4}$$

To test this solution, we used the permeability in a partially saturated sample obtained from steady-state measurements (e.g., Jones and Owens[9]) together with known porosity, sample dimensions, nitrogen viscosity and compressibility, and the value of the downstream volume, V_2, to calculate the decay curve based on Equation 3.3 (see Figure 3.3). The experimental pressure-decay curve for the same sample under the same conditions also is shown in Figure 3.3. For comparison, we also calculated a decay curve based on the simplified analytical solution of Zoback and Byerlee. That solution predicts an exponential pressure decay of the form

$$P_1 - P_p(L,t) = (P_1 - P_2^o) \cdot e^{-mt} \quad , \tag{3.5}$$

where $m = A/ LV_2$. The agreement between the actual decay curve and that predicted by the error-function solution is considered excellent and is convincing evidence of our solution's validity. The exponential decay curve, however, does not predict accurately the actual decay, particularly at early times. In this case, if the exponential solution were used to calculate permeability, the result would be about 20% too small. More significant errors can occur with the exponential solution, however, if the pore volume is either much larger or much smaller than the storage volume V_2. A further problem with the exponential solution is that it fits only the real decay curve at later times; therefore, it takes longer to record a given pulse decay. This may be a significant factor at very low permeabilities, where decay times can be several hours.

Because Equation 3.3 cannot be solved explicity for k, we have written a shore computer program to find the value of k that provides the best agreement between Equation 3.3 and the experimentally determined pulse decay.

EXPERIMENTAL RESULTS

Confining Pressure

The effect of confining pressure on the permeability of dry (S_2=0) samples is shown in Figures 3.4 and 3.5. Considerable hysteresis was observed in all samples during the first confining-pressure cycle but little or now hysteresis was observed in later cycles. The data show strong dependence on confining pressure, particularly at low pressures where open microcracks allow considerably more flow. Obviously, standard air-permeability methods, which use very low confining pressure, would give seriously inaccurate values for these samples.

Confining Pressure, Pore Pressure, and Saturation

We also measured permeability as a function of confining pressure at various degrees of water saturation. The water is initially distilled, deionized, and deaerated, and then is combined with 1 wt% KCl to minimize clay expansion and migration in the rock. Data for permeability vs. confining pressure in Sample SR 6521 at 0 and 48% saturation are shown in Figure 3.6, together with a best-fit, first-degree polynomial. The value of permeability at 45 MPa confining pressure (k_{ref}) was found from this polynomial.

Note that the sample is more sensitive to confining pressure when S_w>0. Measurements at 24, 26, and 60% saturation show that the sensitivity to confining pressure (α) increases markedly with S_w, as shown in Table 3.2. The quantity α is defined as $1/k_{ref}(dk/dP_c)$ at constant P_p).

Sample SR 7227 (Figure 3.7) shows much the same behavior with respect to confining pressure. In this sample, we also measured permeability as a function of gas pore pressure (P_p) for S_w=0. The dependence of permeability on pore pressure will be called β and is defined as $1/k_{ref}(dk/dP_p)$ at constant P_c. As shown in Table 3.2, β is almost twice as great as α, indicating that the permeability of this rock is more sensitive to pore pressure than to confining pressure.

In sample SR 6605, α for S_w=0 falls somewhere between Samples SR 7227 and SR 6521, but with increasing water saturation, no significant change in occurs (Figure 3.8). At 50% saturation, we varied pore pressure while holding confining pressure constant and found, as before, that β is greater than α by a factor of about two (Table 3.2).

Saturation Effects

The permeability on a log scale vs. degree of saturation for each sample at in-situ pressures is shown in Figures 3.9 and 3.10. The relative sensitivity to saturation can be appreciated by considering that at 48% saturation the permeability of Sample SR 6605 decreased by a factor of more than five. For the same saturation, Sample SR 7227 drops by a factor of nine and Sample SR 6521 by a factor of almost 40.

DISCUSSION

The results show clearly that confining pressure must be applied to obtain reliable in situ permeability estimates in tight sandstones. Core measurements under low confining pressure give values 5 to 10 times higher than in situ and probably would not be useful even for comparative purposes. For example, in Figure 3.5, Sample SR 6521 has twice the permeability of Sample SR 6605 at 6 MPa effective pressure, but at 35 MPa they are almost equal. Even more important, however, may be pore pressure. In two of the samples tested, pore-pressure variation had twice the effect on permeability as confining pressure.

The large effect that liquid saturation has on gas permeability in reservoir rock is well known. Low-permeability samples, however, are especially dependent on saturation, particularly above 50% water saturation. This fact underscores the need for accurate in situ S_w determination in tight formations. For example, the difference in permeability between 26 and 48% saturation is a factor of eight in Sample SR 6521. Such sensitivity may have important implications in drilling and fracturing of formations where the injection of fluids may cause serious water-block problems. Finally, when gas permeability with partial liquid saturation is measured, the compressibility of the pore space should be considered in calculating the degree of saturation. For instance, if Sample SR 7227 is 60% saturated at benchtop conditions, it is 71% saturated when in-situ levels of pressure are applied. The pore-space compaction that causes this relative change in saturation also is responsible for the sample's increased sensitivity to confining pressure when partially saturated. Because capillary forces are strong enough to block small pores to gas flow, the displacement of water

from compacting pores causes blocking of some pore throats -- hence, the effect shown in Figures 3.6 and 3.7.

Finally, it should be emphasized that pulse-decay measurements can give quite reliable permeability information if the theoretical development is done properly. Interpreting the data with a simple exponential decay model can give seriously inaccurate permeability values. Furthermore, because the rate of pulse decay depends on pore volume, the magnitude of error will vary from sample to sample. Also, partial liquid saturation reduces the pore volume available for gas flow, and any interpretation that does not account for this change will give permeabilities with different errors at different saturations.

CONCLUSIONS

These data show that pore pressure and confining pressure have large effects on permeability in tight sands and that water saturation may be one of the most critical factors in determining the recoverability of gas from such formations. We also have shown that the dependence of gas permeability on confining pressure increases with increasing partial water saturation. These findings underscore the need to perform all laboratory measurements on tight sands at in-situ conditions, including elevated confining pressure, pore pressure, and water or brine saturation. Finally, we conclude that the pulse-decay method is a fast and accurate technique well suited to measuring permeability in tight sandstones.

NOMENCLATURE

A = cross-sectional area of sample

$c = k/\mu\beta\psi$

k = permeability

k_{ref} = permeability at in-situ P_p and P_c

L = sample length

P_c = confining pressure

P_p = pore pressure

$P_0 = P_2 - P_1$ or pore-pressure step magnitude

P_1 = pressure in volume V_1 (constant during decay)

P_2 = pressure in volume V_2

P_2^o = pressure in volume V_2 at time zero

S_w = fluid saturation

t = time

u = distance along sample

V_1 = upstream volume

V_2 = downstream volume

$\alpha = (1/k_{ref})(dk/dP_c)$ at constant P_p

β = fluid compressibility $= (1/k_{ref})(dk/dP_p)$ at constant P_c

$\kappa = kA/\beta\mu V_2$

ψ = sample porosity

μ = fluid viscosity

SI METRIC CONVERSION FACTORS

bar x 1.0*	E-01 = MPa
ft x 3.048 000*	E-01 = m

*Conversion factor is exact.

REFERENCES

1 Masters, John A., "Deep Basic Gas Trap, Western Canada," Bull., AAPG (1979) 152-181.

2 Brace, W.F., Walsh J.B., and Frangos, W.T., "Permeability of Granite Under High Pressure," J. Geophysical Research (1968) 2225-2236.

3 Sanyal, S.K., Pirnie, R.M. III, Chen, G.O., and Marsden, S.S. Jr., "A Novel Liquid Permeameter for Measuring Very Low Permeability," Soc. Pet. Eng. J. (June 1972) 206-209.

4 Zoback, M.D., and Byerlee, J.D., "The Effect of Microcrack Dilatancy on the Permeability of Westerly Granite," J. Geophysical Research (1975) 752-755.

5 Miller, F.G., "Theory of Unsteady-State Influx of Water in Linear Reservoirs," J. Inst. Pet. (1962).

6 Lin, W., "Compressible Fluid Flow Through Rocks of Variable Permeability," UCRL-52304, Lawrence Livermore Laboratory, Livermore, CA (1977).

7 Goldstein, S., "The Application of Heaviside's Operational Method to the Solution of a Problem in Heat Conduction," Z. Angew. Math., Mech. (1932) 234- .

8 Carslaw, H.S., and Jaeger, J.C., Conduction of Heat in Solids, second edition, Oxford U. Press, London (1959).

9 Jones, F.O., and Owens, W.W., "A Laboratory Study of Low-Permeability Gas Sands," J. Pet. Tech. (Sept. 1980) 1631-1640.

TABLE 3.1 SAMPLE POROSITY AND MINERALOGY

	Sample 7227	Sample 6521.6	Sample 6605
Porosity	.054	.046	.043
Monocrystalline Quartz	.347	.342	.195
Polycrystalline Quartz	.088	.056	.083
Chert[1]	.209	.124	.345
Feldspar	.005	.005	.014
Argillaceous Grains and Depositional Clay Matrix[2]	.054	.142	.183
Quartz Overgrowth	.108	.100	.062
Dolomite[3]	.104	.152	.050
Calcite[4]	-	-	.025
Siderite	.020	-	-
Unidentified Clay Matrix	.016	.033	-

1. Includes finely crystalline quartz grains with sericite (clay mica).
2. Differentiation between squeezed argillaceous grains and depositional clay matrix is at times difficult.
3. Dolomite includes ankerite minerals.
4. Identification based on Red "S" stain.

TABLE 3.2 EFFECT OF P_c, P_p, AND SATURATION ON PERMEABILITY

Sample/ Reference Pressures	Partial Saturation	K_{ref} (microdarcy)	$\alpha(bar^{-1})$	$\beta(bar^{-1})$
	.0	3.91	-1.8×10^{-3}	3.3×10^{-3}
#7227	.30	0.85	-4.7×10^{-3}	-
P_c=500 bar	.48	0.46	-6.2×10^{-3}	-
P_p-150 bar	.71	0.018	-1.1×10^{-2}	-
	.0	1.41	-6.6×10^{-3}	-
#6521.6	.24	0.49	-7.1×10^{-3}	-
P_c=450 bar	.36	0.30	-8.4×10^{-3}	-
P_p=140 bar	.48	0.038	-1.7×10^{-2}	-
	.0	2.04	-3.2×10^{-3}	-
#6605	.36	0.60	-	-
P_c=455 bar	.48	0.38	-	-
P_p=140 bar	.60	0.29	-2.8×10^{-3}	6.4×10^{-3}
	.72	0.128	-	-

k_{ref}=permeability at reference pressures $\alpha = (\frac{1}{k_{ref}}) \cdot \frac{dk}{dP_c}\Big|_{P_p}$; $\beta = (\frac{1}{k_{ref}}) \cdot \frac{dk}{dP_p}\Big|_{P_c}$;

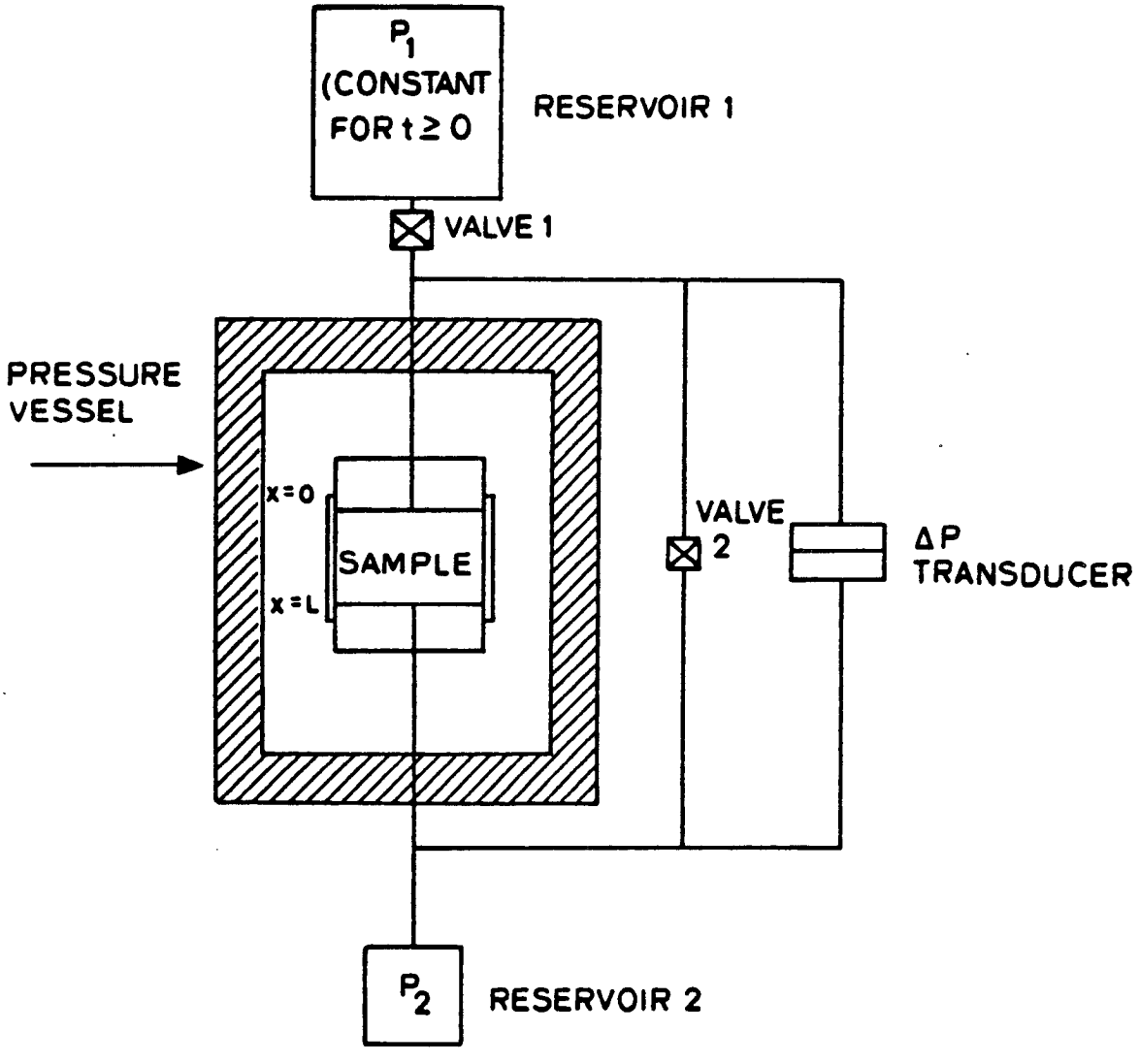

FIGURE 3.1 Schematic of pulse-decay permeameter.

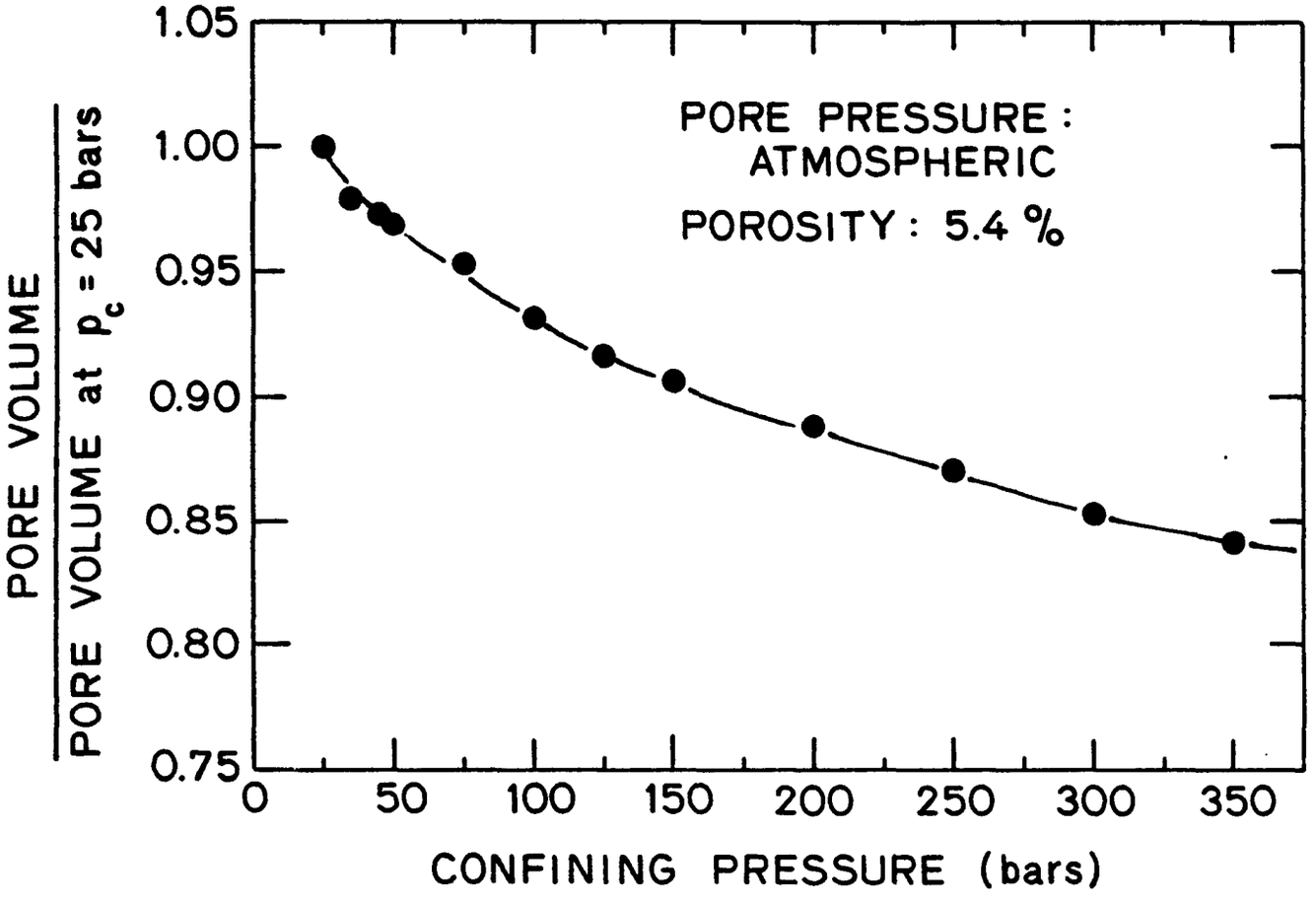

FIGURE 3.2 Pore-volume reduction vs. confining pressure for Sample SR 7227.

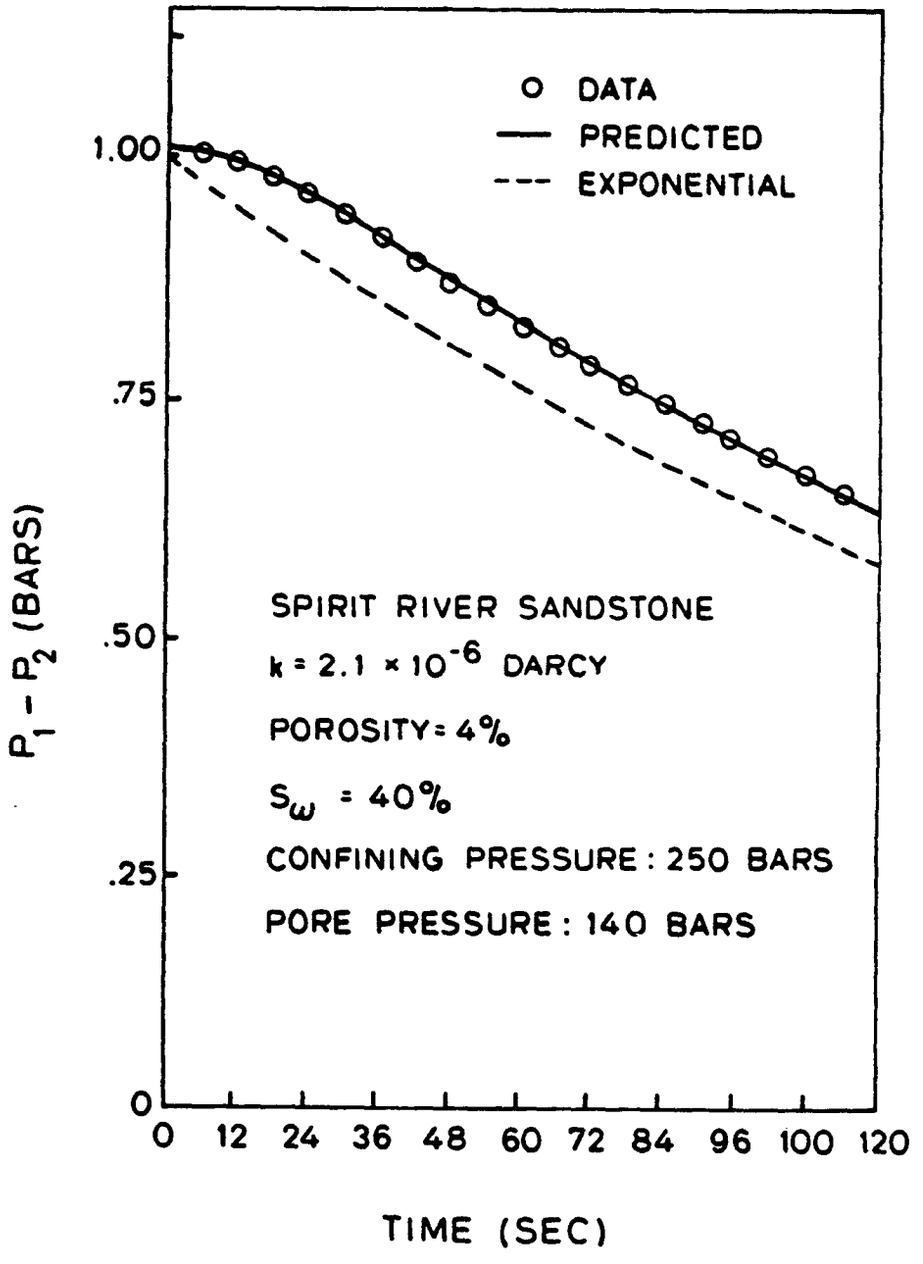

FIGURE 3.3 Theoretical and experimental pulse-decay curves.

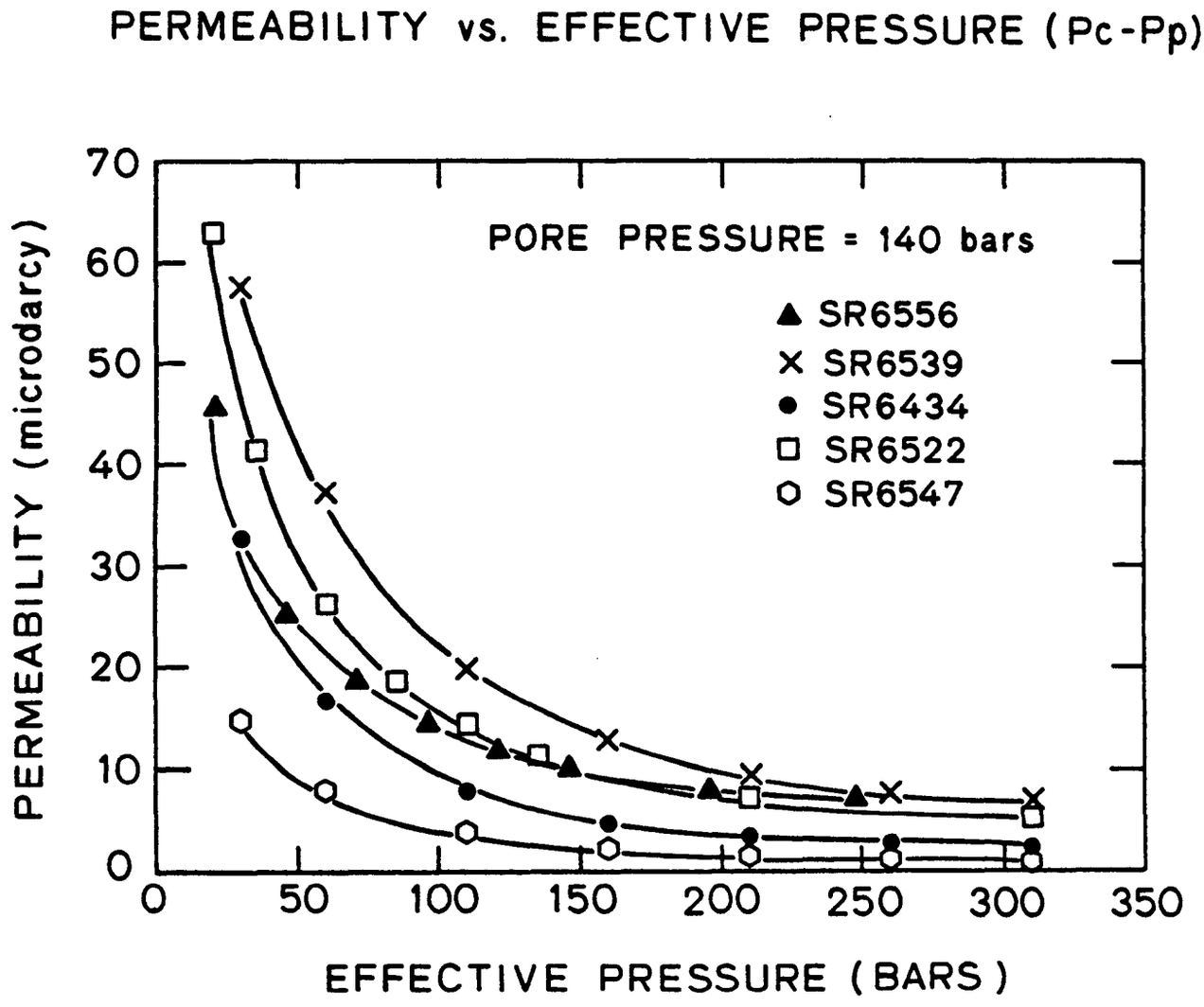

FIGURE 3.4 Gas permeability vs. effective pressure at zero saturation.

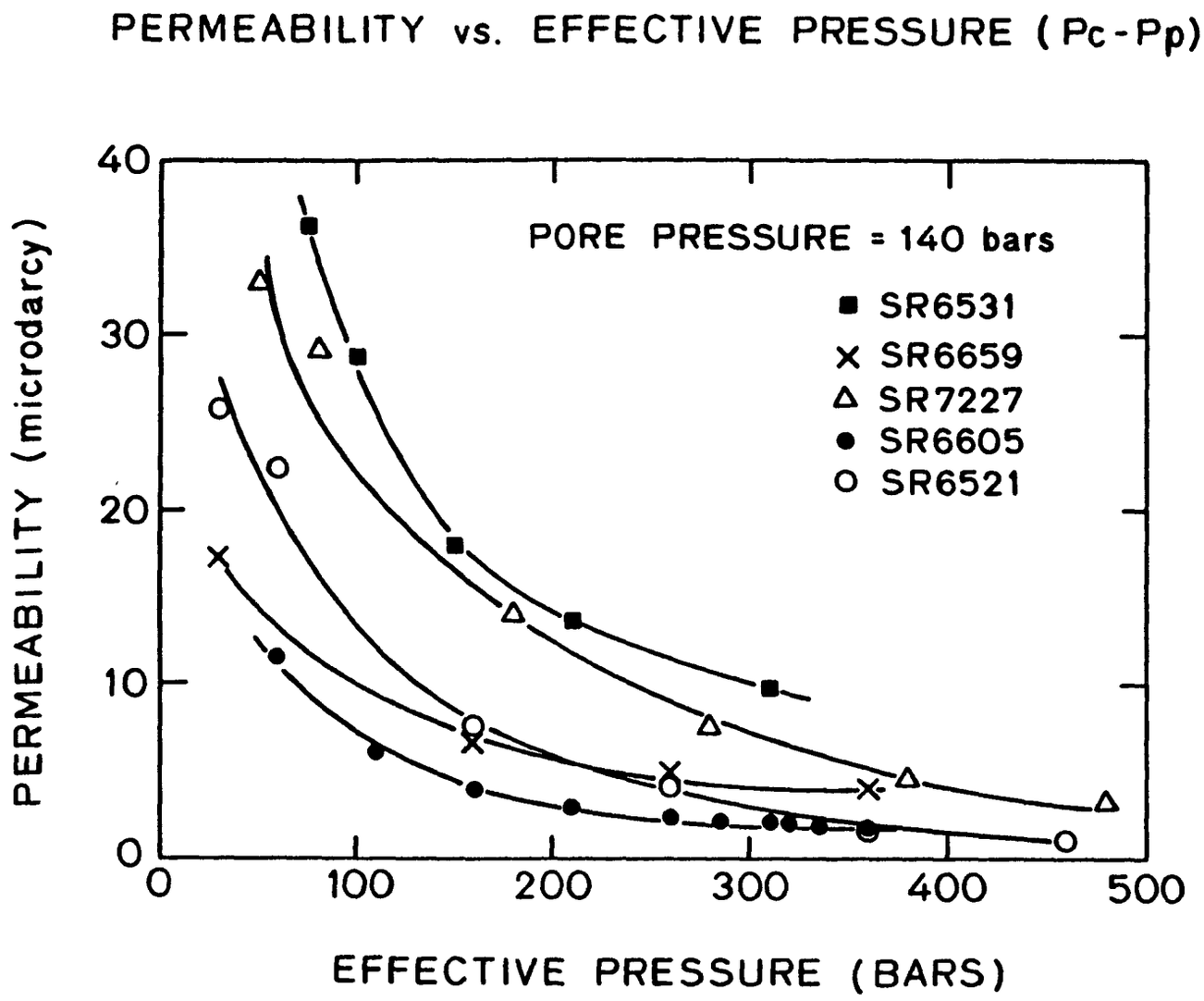

FIGURE 3.5 Gas permeability vs. effective pressure at zero saturation.

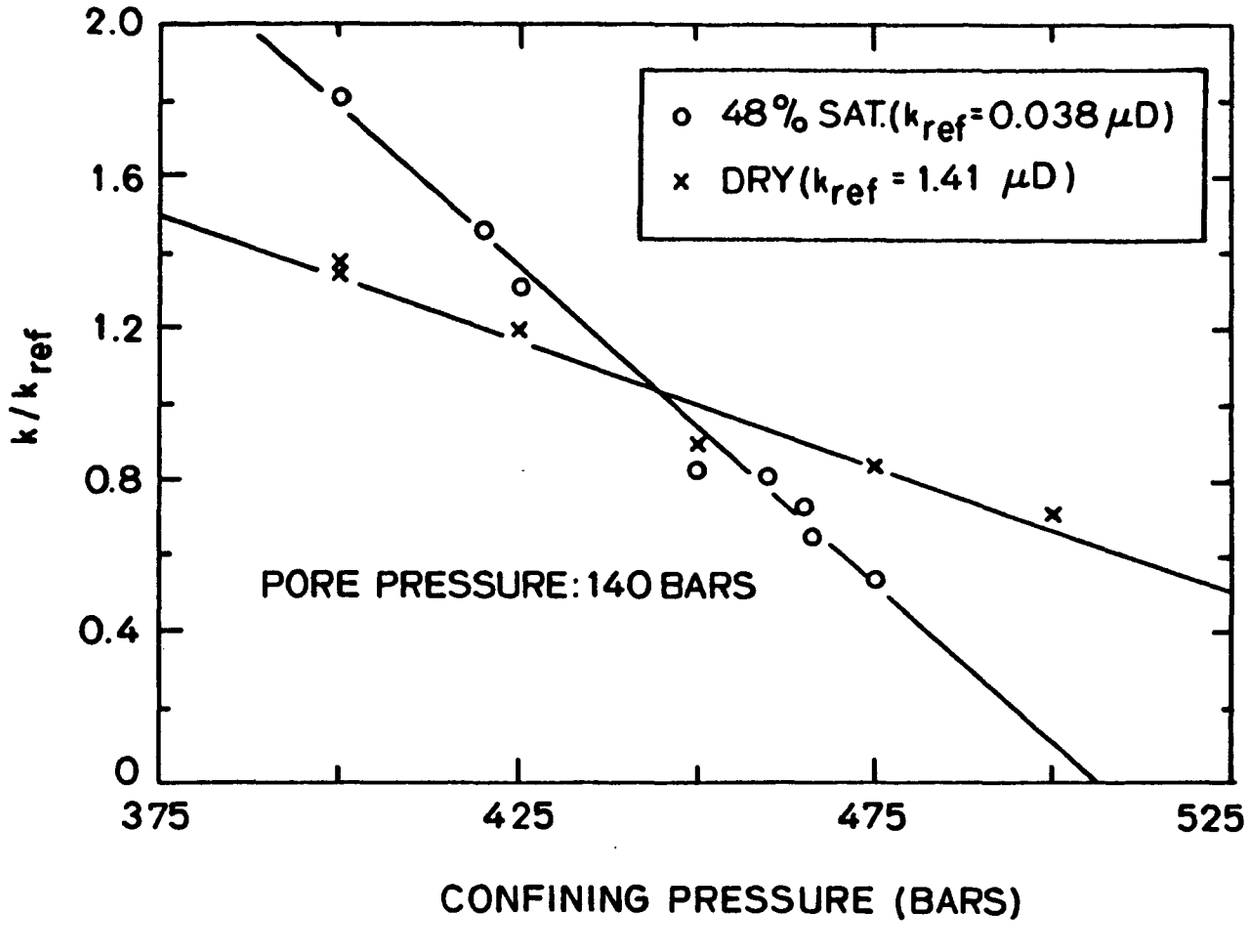

FIGURE 3.6 Gas permeability vs. confining pressure for Sample SR 6521, dry and partially saturated.

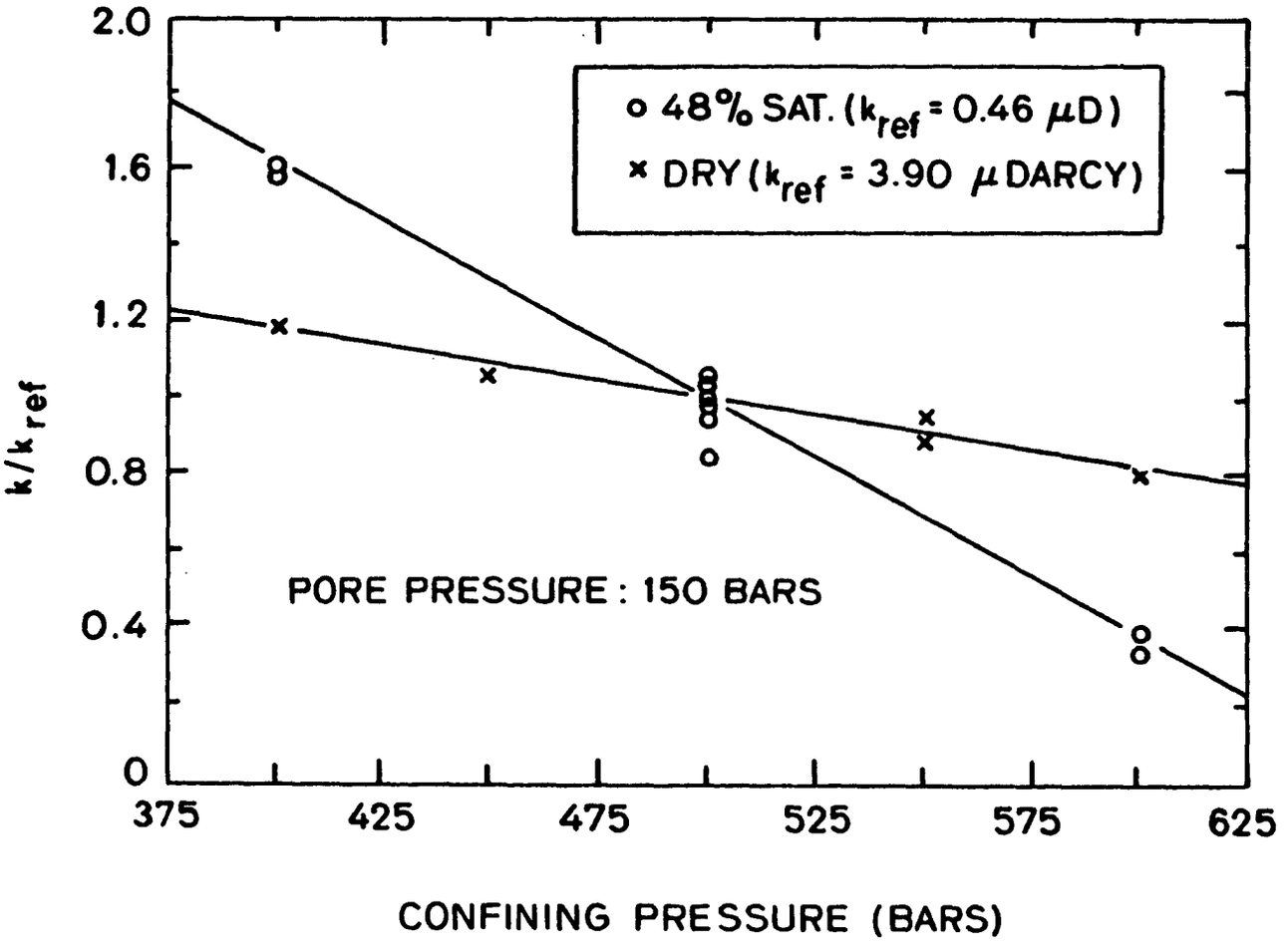

FIGURE 3.7 Gas permeability vs. confining pressure for Sample SR 7227, dry and partially saturated.

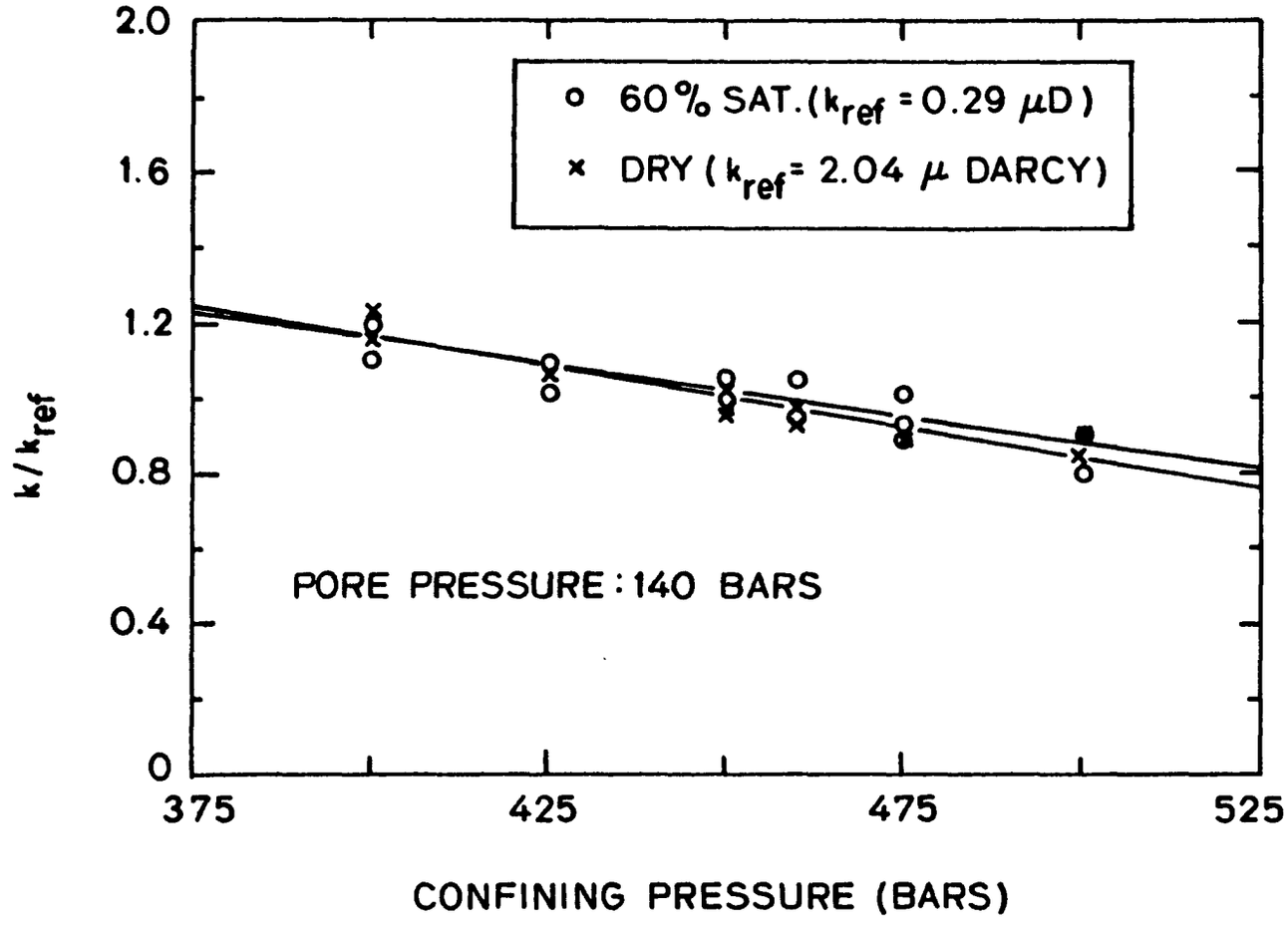

FIGURE 3.8 Gas permeability vs. confining pressure for Sample SR 6605, dry and partially saturated.

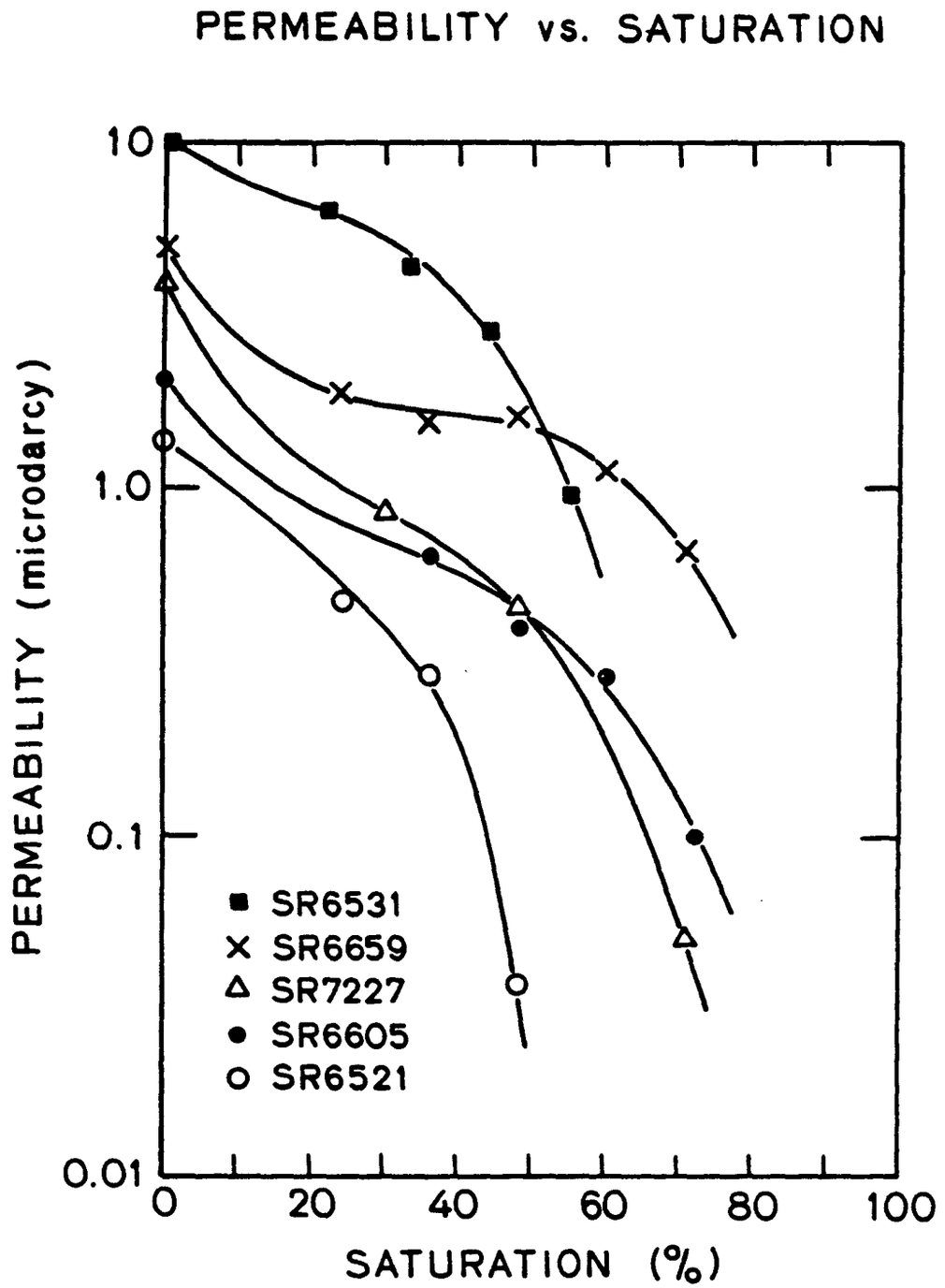

FIGURE 3.9 Gas permeability vs. brine saturation at in-situ P_c and P_p.

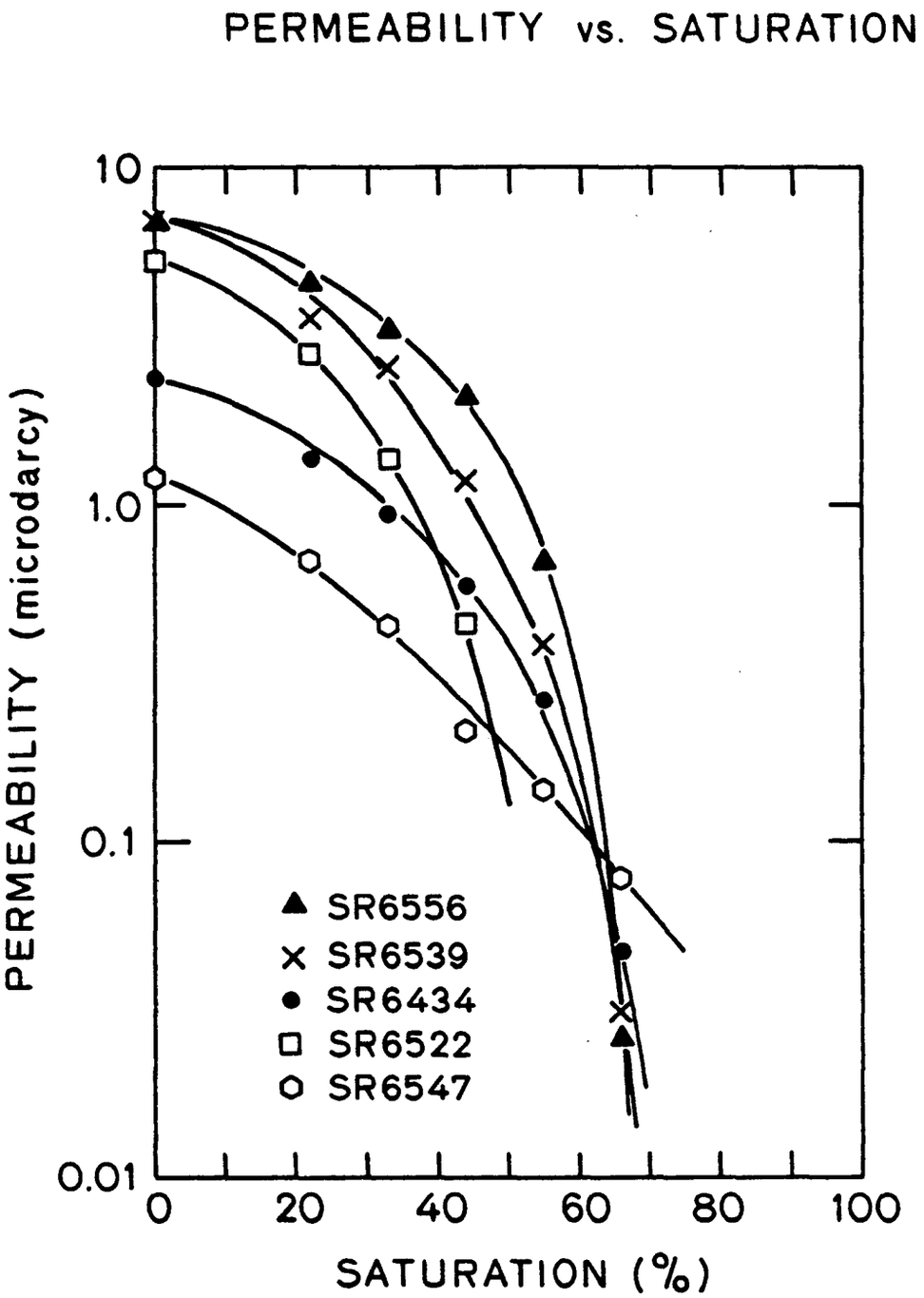

FIGURE 3.10 Gas permeability vs. brine saturation at in-situ P_c and P_p.

CHAPTER 4

TIGHT GAS SANDS:

PERMEABILITY, PORE STRUCTURE AND CLAY

ABSTRACT

Gas permeability has been measured on a suite of cores from the Spirit River tight gas sand of western Alberta and on two samples from the Cotton Valley formation of East Texas. Using nitrogen as the mobile fluid, we have measured permeability as a function of partial water saturation at in situ levels of pore pressure and confining pressure. Samples from both locations show strong dependence of permeability (k) on effective pressure and degree of water or brine saturation. The validity of Darcy's law in the microdarcy range has been verified in a dry Spirit River sample. Extensive thin section, x-ray diffraction and scanning electron microscope (SEM) studies have been conducted. The primary clays in Spirit River and Cotton Valley cores are chlorite and illite. In one sample we measured k vs. saturation first with distilled water and then with a 2% KCl brine solution and saw no significant change in permeability behavior. By observing the effects of pressure, partial saturation and salinity on permeability in these samples, several important characteristics of the pore structure can be deduced and the relative importance of clay content can be evaluated.

INTRODUCTION

Conventional well logging and well stimulation methods have had to be modified substantially to be successful in tight sandstones. It is now clear that there are some fundamental differences in rock-water-gas interactions in these formations as compared to "normal" gas reservoirs. These differences result primarily from significant pore structure alterations as the rock undergoes compaction and diagenesis. In this paper the effect of tight sandstone pore structure on gas permeability will be presented in terms of the response to effective pressure and partial water saturation. Hopefully, some of these results will facilitate the development of well evaluation and stimulation techniques.

We measure nitrogen permeability with a pulse-decay technique which allows independent control of pore pressure, confining pressure and partial saturation. The core sample is about 5 cm in diameter and 6 to 7 cm long. It is jacketed, placed in a confining pressure vessel and subjected to hydrostatic loading of up to 1000 bars. The pore fluid is nitrogen at pressures up to 700 bars. Permeability is measured by applying a 1 bar pore pressure differential across the sample and observing the rate of pressure decay as gas flows through the core. This "pulse decay" can be used to calculate permeability. A complete description of the experimental method is given in Walls, Nur and Bourbie (1980). We have performed several tests to insure the accuracy and repeatability of all measurements and one such test will be described later. The primary advantage of the pulse-decay method is the speed and simplicity of data acquisition as compared to steady-state experiments.

SAMPLE CHARACTERIZATION

Ten of the samples tested were vertical cores from the Spirit River formation in the Deep Basin of western Alberta. The other two samples were horizontal cores from the Cotton Valley formation of East Texas. The mineralogy of these samples as determined from thin section analysis is shown in Table 4.1. Samples are designated by a number corresponding to depth in feet preceeded by SR for Spirit River and CV for Cotton Valley. Scanning electron microscope (SEM) and x-ray diffraction studies indicate that chlorite and illite in approximately equal proportions are the major clay constituents in Cotton Valley samples and illite is the major clay in Spirit River cores. The porosities shown in Table 4.1 were determined by careful weighing of the dry and fully saturated samples.

We have made SEM photographs of most of the samples tested. The photos provide some direct information on pore structure and clay type. Figure 4.1 shows sample CV9380 at two magnifications. The white bar below Figure 4.1a is equal to 100 microns. At this relatively low magnification we can see many flat cracks between quartz grains as well as some rounder pores. Figure 4.1b is a close up of the large pore in the center of Figure 4.1a. We can identify the flaky clay structure as illite with possibly some chlorite. Figure 4.2a is SR6521 at 1000x magnification. Again we can see flat cracks between quartz grains and some open pores with illite coatings. Figure 4.2b shows some of the fragile illite structure at about 4000x magnification. In these photos we have selected areas where clay is clearly present, but it should be emphasized that on a larger scale, quartz is very much predominant in both samples.

EXPERIMENTAL METHODS AND RESULTS

Darcy's Law

To verify that gas flow in these samples obeys Darcy's Law, we conducted a simple experiment, varying only the magnitude of the pore pressure pulse (ΔP). The sample was SR6434, at 140 bars pore pressure, 450 bars confining pressure and with zero water saturation. As expected, the permeability was calculated to be the same at all pressure pulse amplitudes, to within the experimental error (Figure 4.3). This confirms Darcy's law in the microdarcy range, at least for dry samples. A similar test will be conducted on partially saturated samples in the near future. Figure 4.3 also shows that the resolution of the technique is about $\pm$ 8% for each pressure pulse, if the pulse amplitude is 1 bar or greater. In practice we take at least 3 pulse decays for each measurement and average them so that the error is reduced to about $\pm$5%. The data taken at lower pulse amplitudes is more scattered because room temperature fluctuations induce small pressure changes in the system and these become more significant as ΔP is reduced. All measurements presented hereafter were taken with about a 1.5 bars pulse amplitude.

Confining Pressure

Always of great interest in permeability measurements is the effect of overburden or confining pressure on the sample. For each sample we have measured permeability as a function of external hydrostatic confining pressure (P_c) with pore pressure (Pp) held constant at approximately *in situ* levels and with zero saturation. The difference between P_c and Pp is called

effective pressure (P_e). Permeability vs. P_e is shown in Figure 4.4 for three of the Spirit River cores and both Cotton Valley samples. If we let k_{30} be the permeability at P_e = 30 bars and k_{300} be permeability at P_e = 300 bars, we can calculate a reduction factor, k_{30}/k_{300}, for confining pressure. This quantity is between 3 and 15 for all samples measured. A complete list of k_{30}/k_{300} is given in Table 4.2 along with the permeability of each dry sample at in situ P_c and P_p. Significant hysteresis in the k vs. P_e curve was observed only on the first cycle. The data presented here is for downgoing P_e on the second cycle. These results for the Spirit River and Cotton Valley samples agree qualitatively with measurements on other tight sandstones by previous investigators such as Thomas and Ward (1972), Byrnes, Sampath and Randolf (1979), and Jones and Owens (1980).

Effective pressure was reduced only to 30 bars in order to avoid any possible gas leak around the jacket. The jacketing material was teflon and had been sealed against the sample by at least 300 bars effective pressure before P_c was reduced to 30 bars. In a separate experiment, using an aluminum plug with a roughened surface it was determined that 5 bars effective pressure was enough to insure good sealing if the jacket had first been formed to the sample at a higher pressure.

Partial Saturation

To measure k as a function of S_w the samples were first fully saturated, then dried to the desired degree of saturation on a digital balance with 0.01 gm resolution. Full saturation was achieved by placing the cores in a small pressure vessel which was evacuated to 50 microns for 12 hours. The vessel was then flooded with deareated water or brine and pressurized to 150 bars

for an additional 12 hours. The saturant for the Spirit River samples was a 1% KCl solution and for the Cotton Valley samples distilled water was used.

At each partial saturation step, the samples were allowed about 12 hours before permeability was measured. This allows the capillary forces to distribute the water saturation throughout the pore space. The evenness of saturation distribution is therefore controlled by the pore structure of the sample just as it would be *in situ*. The time required for equilibrium was determined by measuring permeability every 30 minutes from when a given degree of saturation had been established. From such data, we found that no significant change in permeability occurred after about 4 hours in most cases.

To further assure that saturation distribution was not affecting permeability, we started with a dry sample and *increased* saturation by immersing it in the saturating solution. Again, we waited 12 hours before permeability measurement. Each increasing saturation value was achieved by further immersion in the brine. As can be seen from Figure 4.5, the permeability is not strongly affected by the direction of saturation change. The one exception is at 50% saturation where permeability is somewhat lower on the "absorption" curve than on the "evaporation" curve. We believe this is due to differences in distribution on the pore size scale. Because of capillary hysteresis effects, different pores and pore interconnections are water filled when the sample absorbs water as opposed to when it loses water through evaporation.

Figures 4.6 and 4.7 show the results of changing saturation on gas permeability for the ten samples studied. All the data was taken at approximate *in situ* pore pressure and confining pressure. The saturation values were corrected for pore compressibility effects and are accurate to ±2%.

Parts of the saturation curve for SR6434 had to be repeated because of equipment problems. Figure 4.8 shows the agreement between the original data and that taken at a later time is quite good. Note that the two dry data points are essentially identical, which means no permanent change in permeability resulted from the saturation process.

Confining Pressure and Saturation

To see what effect partial saturation would have on the confining pressure dependence of a tight sandstone, we measured k as a function of P_c for sample SR6522, first at 40% distilled water saturation, then with no saturation. In the 40% saturation case, the drop in permeability with confining pressure was so rapid that a linear plot of k vs. P_c was not desirable. Therefore, the data was normalized to the k value at 20 bars effective pressure (k_{20}) and plotted as the log of k over k_{20} (Figure 4.9). The sample is clearly more sensitive to confining pressure changes when partially saturated than when dry.

Salinity

Two permeability vs. saturation experiments were performed on SR6522 to see what effect, if any, using a KCl solution as the saturant would have after first using distilled water. This sample had very low permeability at 50% H_2O saturation. The first measurable gas permeability was thus at 44% saturation. The sample was then dried to levels of 33%, 22% and finally zero saturation. Permeability was measured at each level at *in situ* pore pressure and confining pressure. Next, the sample was resaturated with a 1% KCl

solution. The permeability measurements were repeated at the same saturations and the results of both tests are shown in Figure 4.10.

DISCUSSION

The behavior of tight gas sand permeability in response to changing confining pressure can be explained qualitatively by the complex and tortuous pore structure which results from extensive compaction and diagenesis. Thin-section and SEM images of the pore structure always reveal very narrow slit-like apertures between pores. These thin cracks provide the major connectivity which allows fluid to move when the rock is under low effective pressure conditions. However, such flat cracks are easily closed by increasing overburden pressure (Walsh and Brace, 1966) and their effect on permeability can be seen in Figure 4.4. At higher P_c their contribution to flow has been almost eliminated and permeability is provided by the rounder cross-section channels. This behavior explains why permeability measured with only a few bars confining pressure is not representative of the in situ permeability (Wyman et al., 1980).

The effect of partial saturation on gas permeability is also largely controlled by pore structure. Water tends to collect in small pores and cracks due to capillary forces and thereby prevents those channels from transmitting gas, unless the pressure gradient is sufficiently large to cause water displacement. Jones and Owens have shown that it takes several hours to reduce a fully saturated Spirit River core to 40% saturation using a 27 bar/cm gas pressure gradient. Since the gradient in our pulse decay experiments is about 0.25 bar/cm, we would not expect any significant water movement. This is confirmed by weighings before and after permeability measurements which show no saturation change. The large gas pressure gradient which is required to displace water may be partially responsible for the failure of some hydraulic fracturing operations to improve well

performance. The fracturing fluid itself invades the formation to some extent, thereby creating a zone of almost zero gas permeability on each side of the fracture. This same "waterblock" phenomenon, on a much larger scale, is believed to be the trapping mechanism for huge volumes of gas in the Deep Basin on Alberta (Masters, 1979).

It is clear from Figure 4.8 that the addition of 40% water saturation increases the sensitivity of permeability to confining pressure. Again, the explanation is derived from pore structure. For the dry rock, flat cracks rapidly close at low pressure until they are an insignificant part of the total flow. Some may even become dead end pores. In any case, at higher pressure, only the more equidimensional pores and channels remain and hence the flattening of the k vs. P_c curve at around 300 bars. When the sample is partially saturated gas flow through flat cracks is impeded more severely by increasing P_e because the water volume remains constant as the crack volume decreases which causes blocking of the pore. However after the crack is fully blocked by water it continues to close with pressure. The water is displaced into the rounder pores and reduces the flow in these channels. The result is a continuing decrease in k even at 300 bars effective pressure. We must also consider that about 10% of the pore volume is lost in going from 30 bars to 300 bars effective pressure so the water saturation increases from 40% to 44% of pore volume.

Even though we are just beginning to study carefully the clays and their effect on permeability we will describe one experiment which sheds some light on the subject. A Spirit River sample has been photographed with the SEM before and after permeability measurements in which a 1% KCl solution was used as the saturant. Figure 4.11a shows a typical portion of the rock where illite is present. The usual flaky, fragile structure of the clay is quite

obvious. Figure 4.11b shows a typical view of the same sample after the permeability measurements with KCl solution saturation. The structure of the clay particles is totally different and appears only as small blocks and globules. Both these samples were scrutinized at length and none of the flaky illite appears in the post-saturation sample nor is the blocky structure visible in the pre-saturation rock. This apparent change in clay structure was sufficient reason to suspect that some change in permeability might also be occurring.

A second Spirit River sample was prepared and the data in Figure 4.10 was collected. This plot shows that no significant change in gas permeability occurs when switching the saturant from distilled water to the KCl solution. So, even though a change in clay morphology was observed, no significant permeability change resulted. The explanation for the clay change is still unclear. There is no apparent reason for the KCl saturant to have such an effect. The sample was dried at about 60°C so temperature should not have been a factor. Further SEM studies on tight sandstones subjected to various saturants is obviously required. Also, additional gas permeability studies with different samples and saturating fluids are necessary to fully understand how clay affects permeability in these samples. A comparison was made between the amount of clay detected by thin section and the severity of the permeability reduction caused by 40% saturation with the KCl solution. Absolutely no correlation was observed. The data now available suggest that clay is not a dominant factor in the permeability of the Spirit River samples. The Cotton Valley cores have, in general, less clay than Spirit River.

CONCLUSIONS

Although the results presented here are not complete, some fairly clear trends have emerged and certain general conclusions are justified for the samples studied.

1) Gas flow in these samples is apparently obeying Darcy's Law.
2) Effective pressure has a large effect on gas permeability below 100 to 200 bars but becomes less important at higher pressures.
3) Partial water (or brine) saturation is of very great importance, particularly above 40% of pore space where most samples show a very steep rate of permeability decline.
4) At 40% saturation, effective pressure causes significant permeability reduction up to and beyond 300 bars.
5) Pore structure seems to be the major factor in determining permeability behavior with clay content being of secondary importance, at least in these samples.

The future direction of this research will be i) to improve the experimental system, permitting faster data collection, and ii) to develop pore network theories which offer the possibility of relating permeability to acoustic and electrical properties. Hopefully, this integrated effort will result in a better understanding of tight gas sands, leading eventually to improved interpretation of borehole logs and other field techniques.

NOMENCLATURE

k = gas permeability

P_c = confining pressure

P_e = effective pressure ($P_c - P_p$)

P_p = pore pressure

ΔP = pore pressure pulse amplitude

SI METRIC CONVERSION FACTORS

1 bar = 10^5 Pa

1 Darcy = 0.9869233 m^2

1μ Darcy = 9.969233 x 10^{-7} m^2

REFERENCES

1 Byrnes, A.P., K. Sampath and P.L. Randolf, 1979, Effects of pressure and water saturation on permeability of western tight sandstones, presented to the Fifth Annual DOE Symposium on Enhanced Oil and Gas Recovery and Improved Drilling Technology, Tulsa, Oklahoma, Aug 22-24.

2 Jones, F.O., and W.W. Owens, 1980, A laboratory study of low permeability gas sands, J. Petr. Tech., 32, 1631-1640.

3 Masters, J.A., 1979, Deep Basin gas trap, western Alberta, Amer. Assoc. Petr. Geol. Bull., 63, 152-181.

4 Thomas, R.D., and D.C. Ward, 1972, Effect of overburden pressure and water saturation on gas permeability of tight sandstone cores, J. Petr. Tech., 24, 120-124.

5 Walsh, J.B., and W.F. Brace, 1966, Elasticity of rock: a review of recent theoretical studies, Rock Mech. Eng. Geol., 4, 283.

6 Walls, J.D., A.M. Nur and T. Bourbie, 1980, Effects of pressure and partial water saturation on gas permeability in tight sands, presented to the 55th Annual Fall Meeting of the Soc. of Petr. Engr., in Dallas, Texas, Sept. 21-24.

7 Wyman, R.E., S.A. Holditch and P.L. Randolph, 1980, Analysis of an Elmworth hydraulic fracture in Alberta, J. Petr. Tech., 32, 1621-1630.

TABLE 4.1 SAMPLE MINERALOGY FROM THIN SECTION*

	SR6531	SR6521	SR6522	SR6539	SR6547	SR6556	SR6605	SR6659	SR6434	SR7227	CV9380	CV9594
Porosity	0.070	0.046	0.079	0.072	0.052	0.074	0.043	0.034	0.054	0.054	0.061	0.051
Quartz	0.446	0.398	0.363	0.379	0.343	0.488	0.270	0.322	0.384	0.414	0.729	0.719
Chert	0.123	0.124	0.112	0.155	0.078	0.133	0.353	0.180	0.196	0.230	0.030	0.030
Feldspar	--	0.005	--	0.012	--	--	0.014	--	--	0.005	0.060	0.020
Argillaceous Grains	0.082	0.142	0.097	0.040	0.032	0.019	0.158	0.092	0.036	0.054	--	--
Dolomite	0.124	0.152	0.156	0.121	0.073	0.095	0.050	0.132	0.112	0.104	--	0.010
Calcite	--	--	--	--	--	--	0.025	0.064	--	--	0.040	0.040
Siderite	--	--	--	0.030	0.301	0.038	--	0.060	0.052	0.020	--	--
Quartz Overgrowth	0.148	0.100	0.152	0.155	0.106	0.143	0.062	0.116	0.155	0.108	0.070	0.120
Unidentified Clay Matrix	0.007	0.033	0.041	0.036	0.015	0.029	0.025	--	0.011	0.011	0.010	0.010

*Porosities measured by saturation technique

TABLE 4.2 PERMEABILITY AND CONFINING PRESSURE SENSITIVITY

Sample	Approximate in situ pressures p_c (bars)	p_p (bars)	Dry k at in situ p_c & p_p (microdarcy)	k @ 30 bars p_e / k @ 300 bars p_e
SR6521	450	140	1.41	13.9
SR7227	500	155	3.91	5.5
SR6605	450	140	2.04	8.0
SR6659	450	140	4.85	3.8
SR6434	450	140	2.38	13.8
SR6547	450	140	1.23	12.3
SR6531	450	140	10.30	--
SR6539	450	140	7.18	8.1
SR6556	450	140	7.11	5.2
CV9380	650	290	3.59	3.2
CV9594	660	300	1.11	3.9

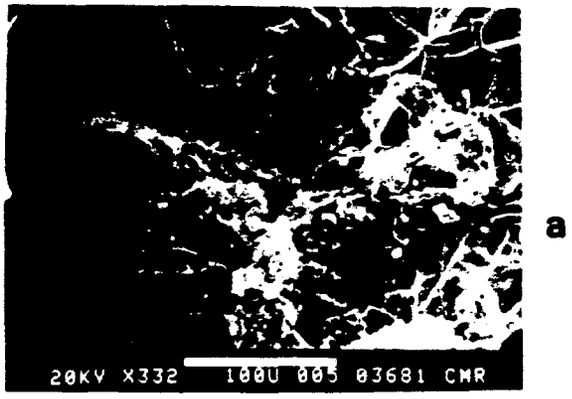

a

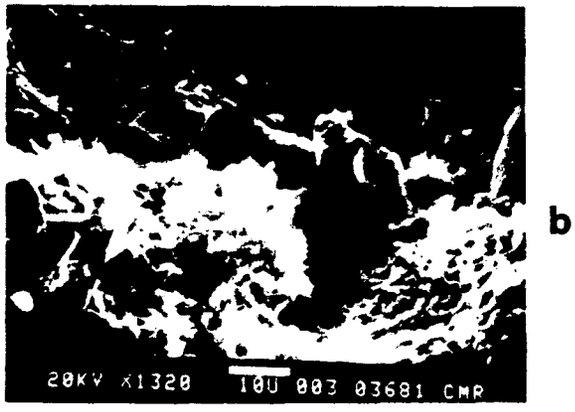

b

Fig. 4.1 SEM photos of Cotton Valley sample 9380.

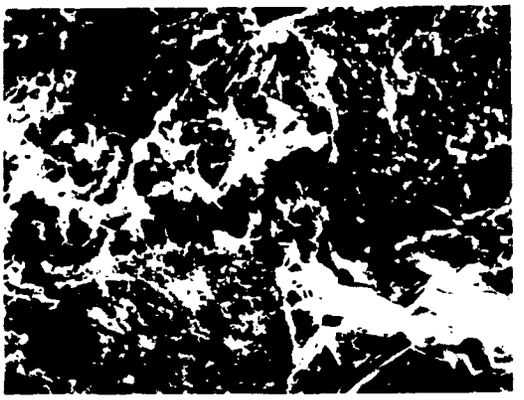

a

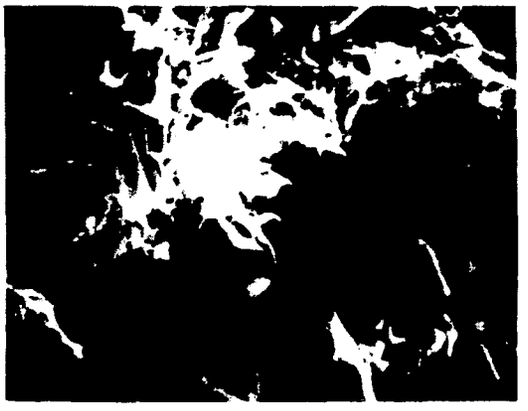

b

Fig. 4.2 SEM photos of Spirit River sample 6521.

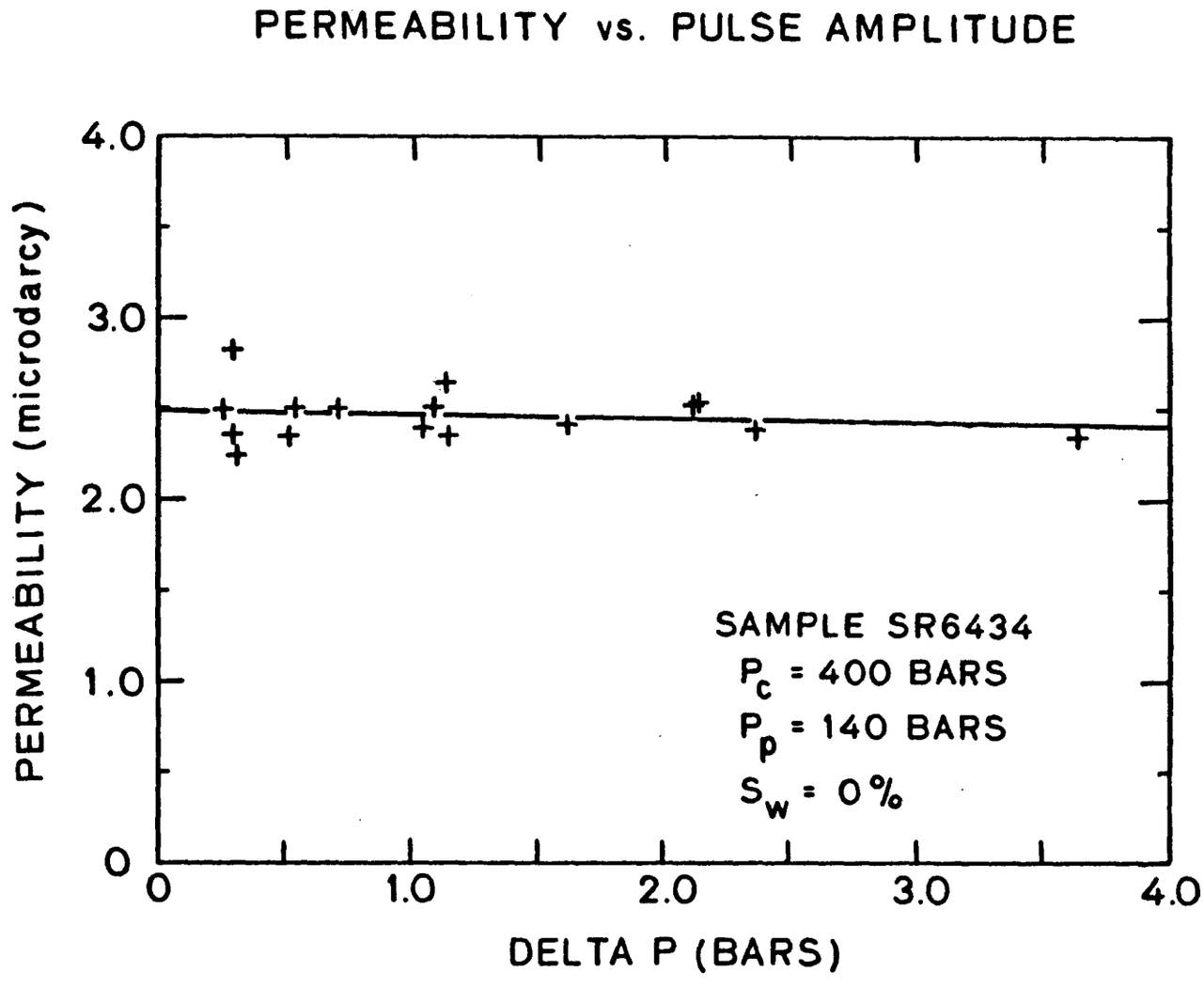

FIGURE 4.3 Verification of Darcy's Law in sample SR 6434 with zero saturation.

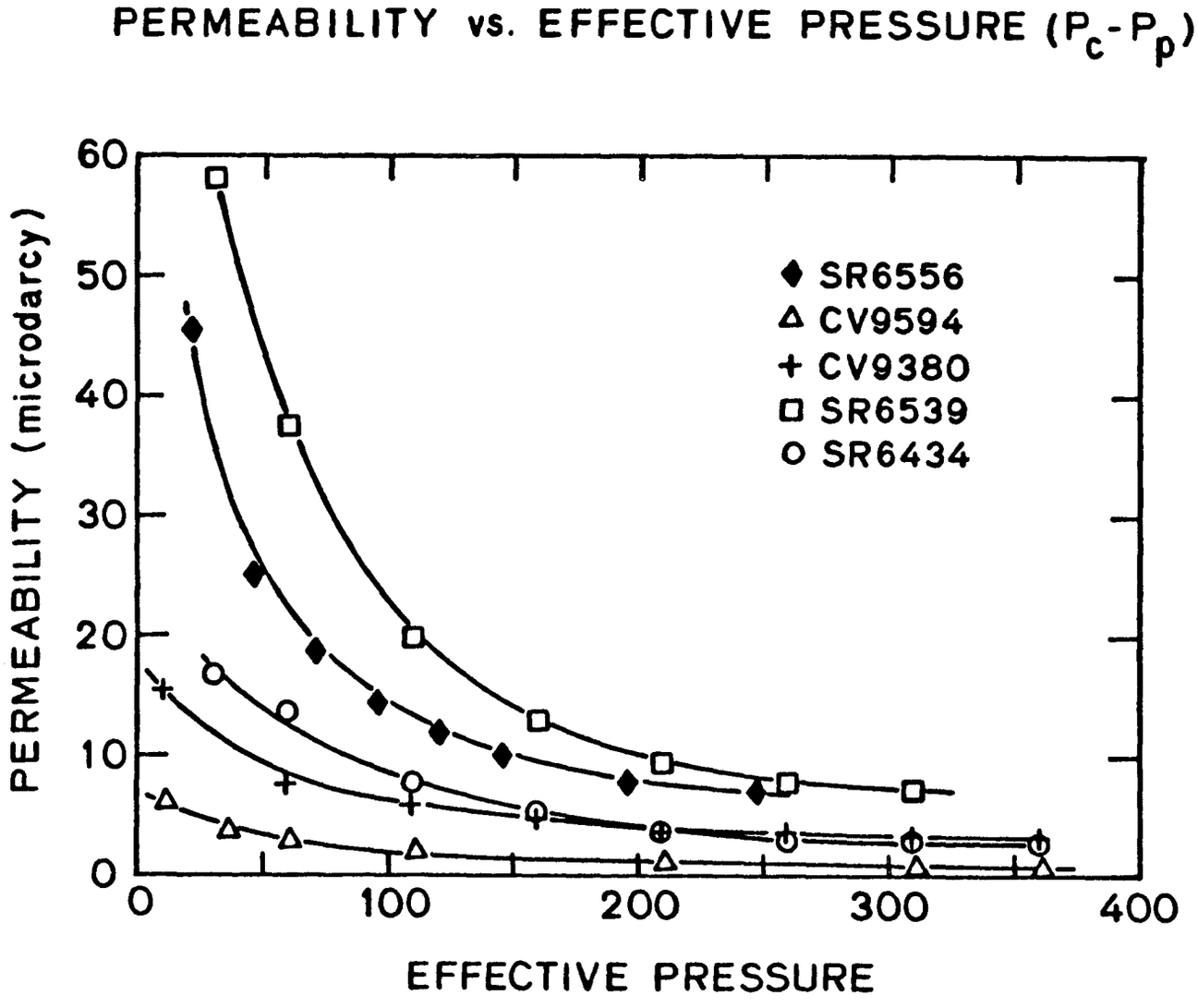

FIGURE 4.4 Effect of confining pressure on some typical tight sandstone.

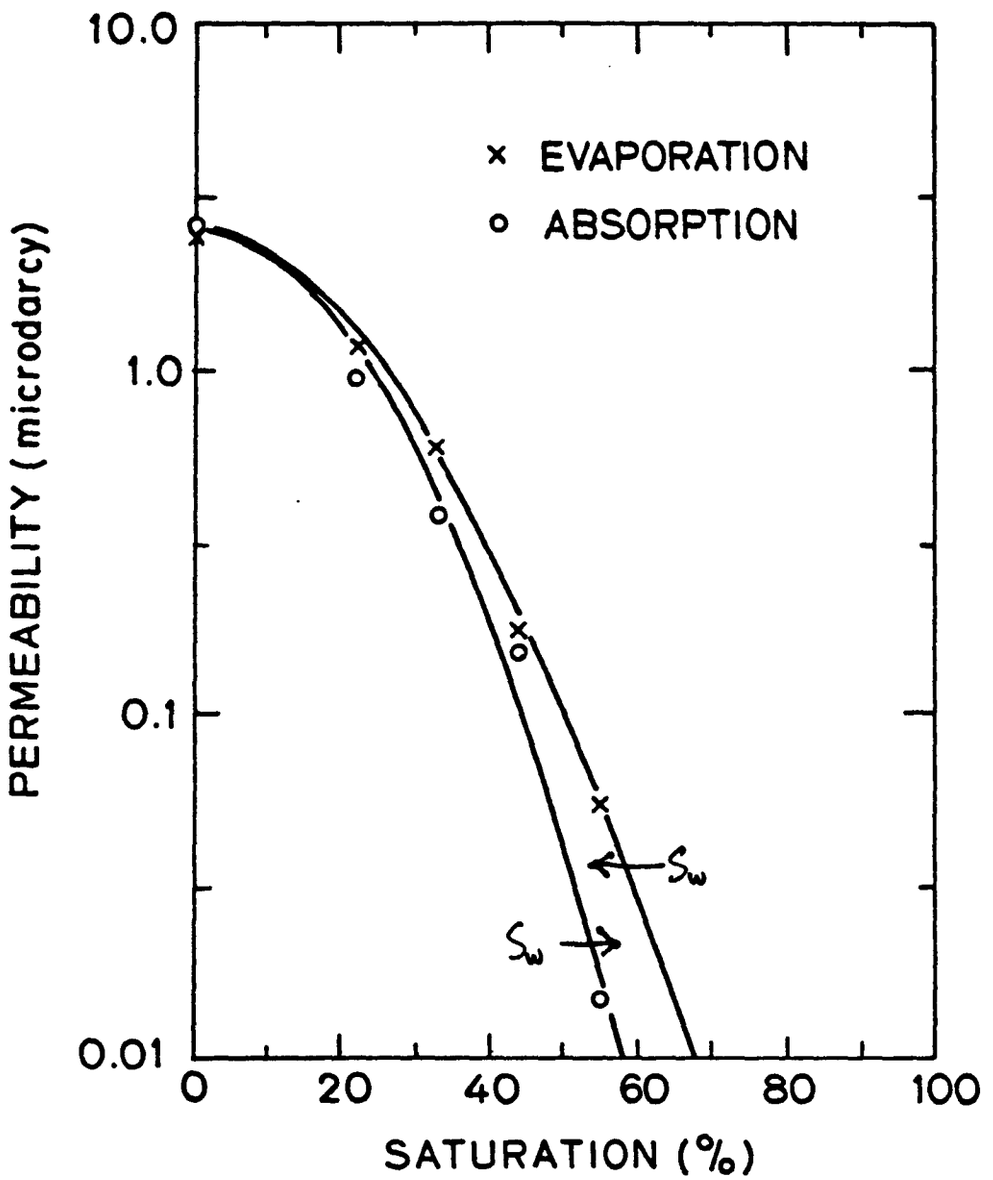

FIGURE 4.5 Gas permeability with two different saturation techniques.

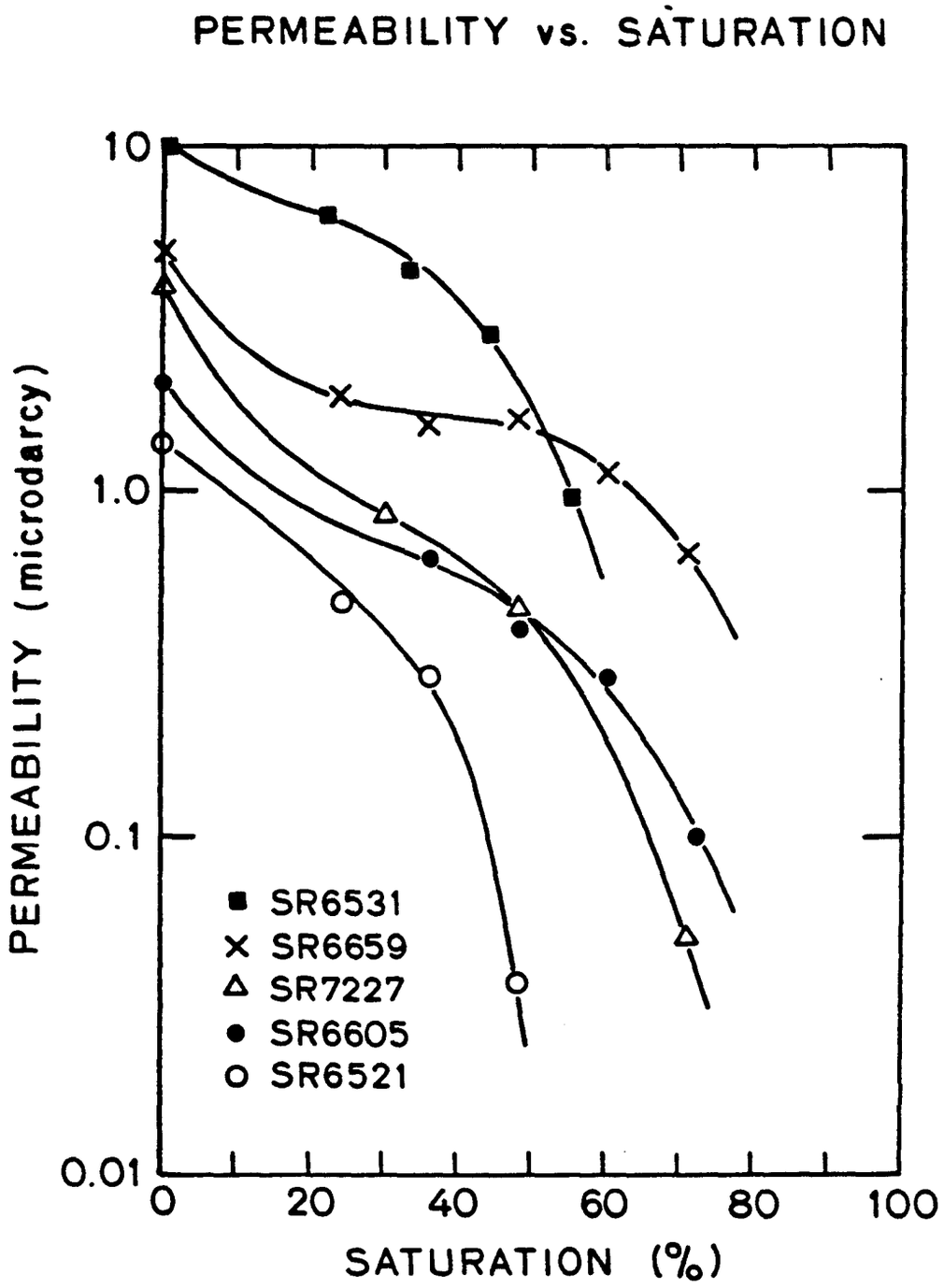

FIGURE 4.6 Effect of partial saturation on permeability in some Spirit River cores.

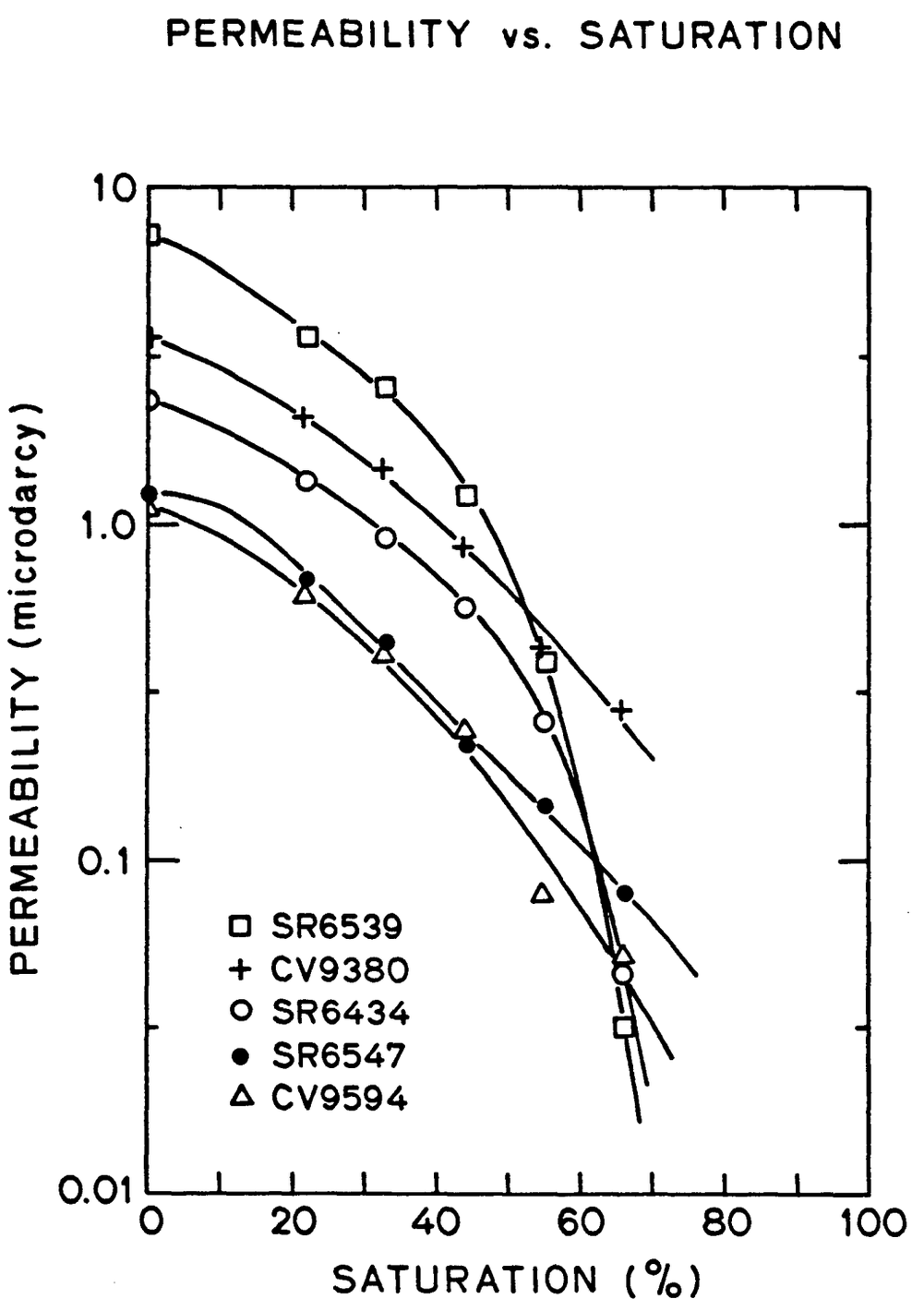

FIGURE 4.7 Effect of partial saturation on permeability in Spirit River and Cotton Valley cores.

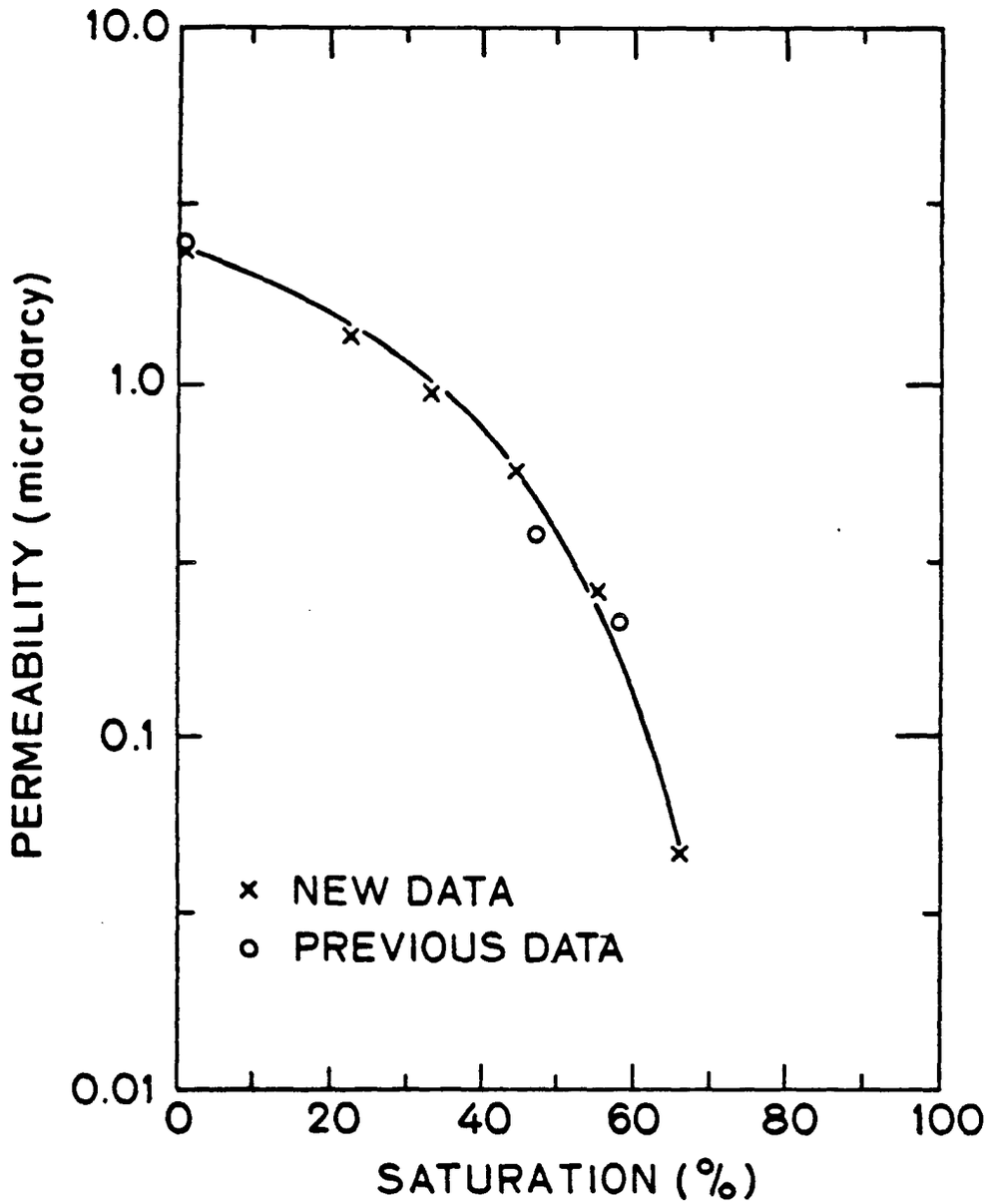

FIGURE 4.8 Reproducibility of k vs. saturation data in SR 6434.

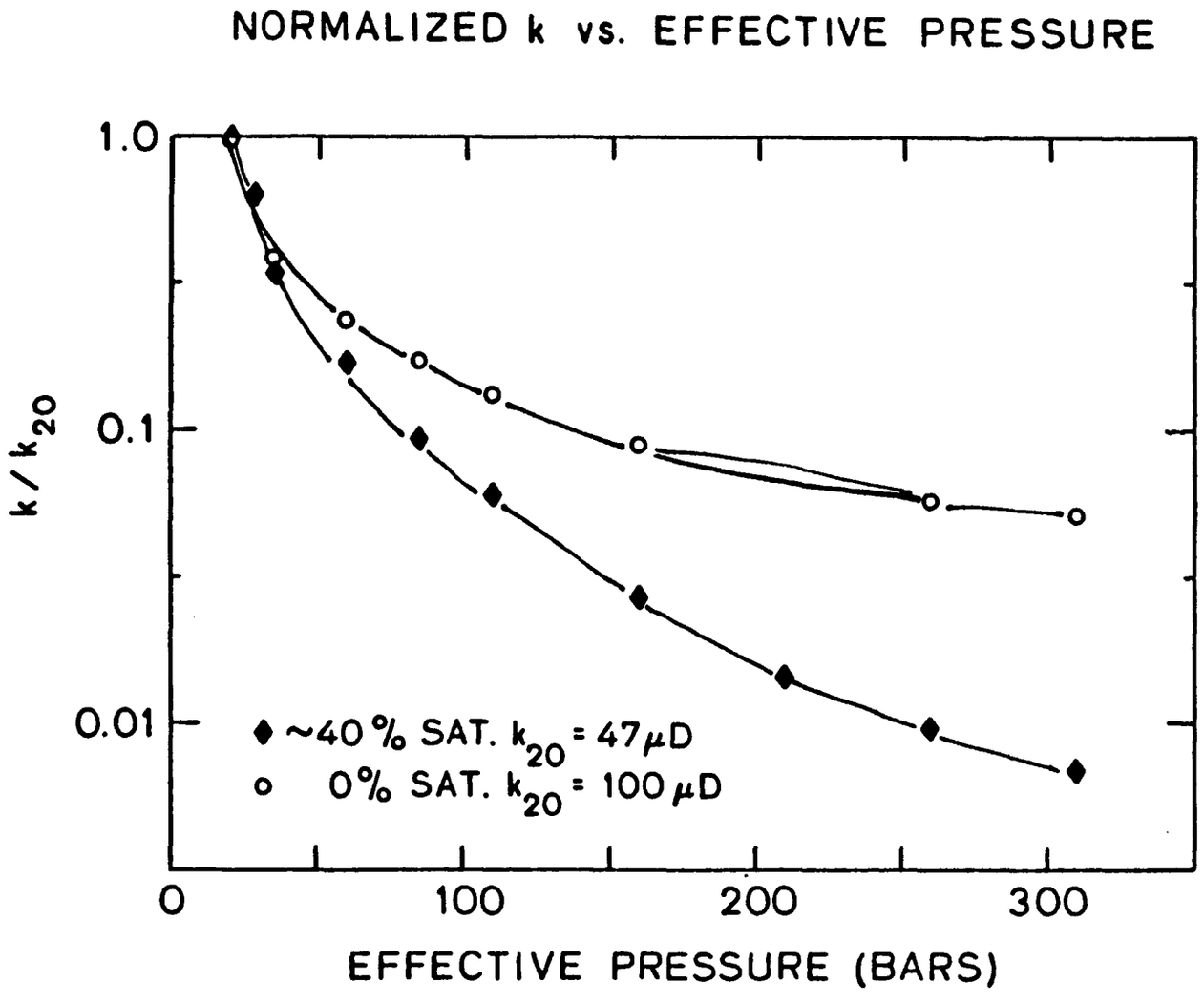

FIGURE 4.9 Effect of confining pressure on dry and partially saturated SR 6522.

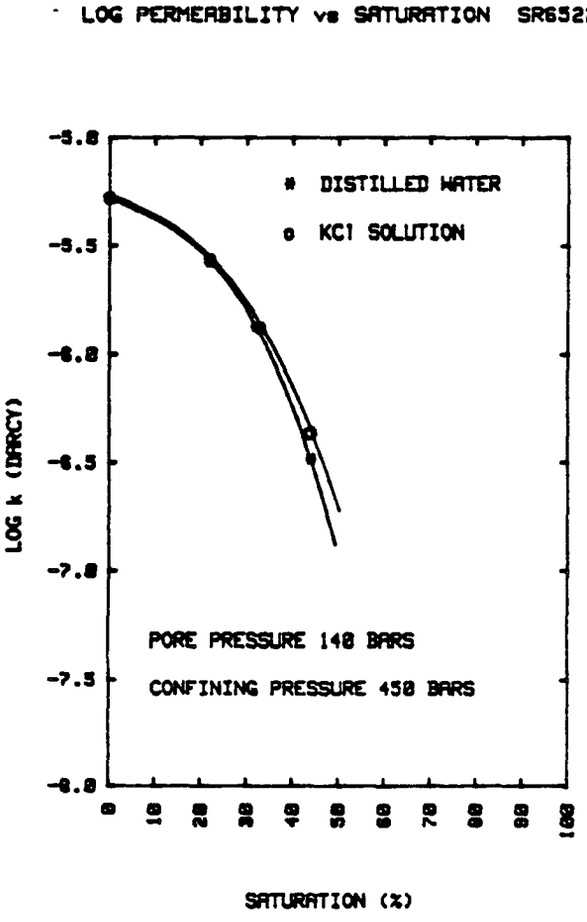

FIG 4.10 Effect of 2% KCl solution after distilled water saturation.

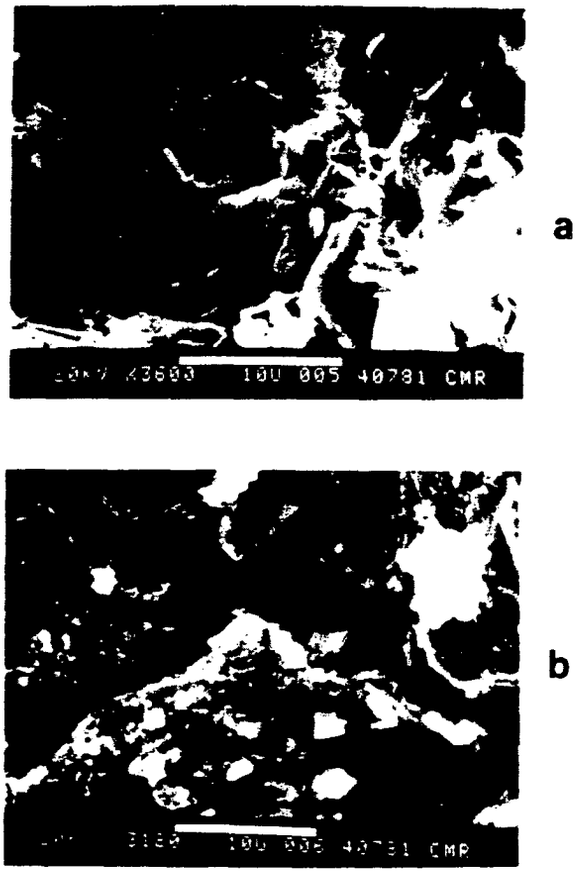

Fig. 4.11 SEM photos of SR6434; (a) before saturation; (b) after 2% KCL saturation.

CHAPTER 5

MEASUREMENT OF FLUID SALINITY EFFECTS ON TIGHTS SANDS WITH A COMPUTER CONTROLLED PERMEAMETER

ABSTRACT

A completely computer controlled pulse-decay permeameter has been designed and constructed. This system can rapidly and accurately measure gas permeability on five samples simultaneously. The samples can be partially saturated with brine or oil and can be placed under confining pressure up to 100 MPa (15,000 psi) and pore pressure to 70 MPa (10,000 psi). The range of permeabilities measurable is 10^{-8} m^2 (0.00001 md) to 10^{-3} m^2 (1 md).

To determine the effect of different brine mixtures on tight gas sand permeability, we saturated five adjacently cut Spirit River sandstones with five different fluids; distilled water, 5% NaCl, 10% NaCl, 1% KCl and 5% KCl. The samples were dried to 66% saturation and gas permeability was measured under in situ pore pressure and confining pressure. This process was repeated, with appropriate equilibration time, for 55, 44, 33 and 22% saturation. The gas permeability vs. saturation curves are very similar, indicating that the samples are not sensitive to the type of fluid in the pores. This can be important in selecting fluid compositions for fracturing procedures. Scanning electron microscope photos of the samples made before and after saturation show no change in the structure of the clays which were primarily chlorite and illite.

INTRODUCTION

In recent years, many rapid advances have been made in the evaluation and development of tight gas sand reservoirs. Most notable are the major achievements in massive hydraulic fracturing and subsequent pressure transient testing. Most major oil companies and many smaller firms are actively involved in developing various tight gas fields throughout the United States and Canada. Estimates by the Gas Research Institute[1] indicate that with advanced technology and favorable prices, U.S. natural gas reserves could double as a result of tight gas sand developments, and that up to 10 trillion cubic feet (TCF) of gas per year could be produced from these formations.

In spite of the significant progress in most areas of tight gas technology, however, little has been done to improve routine core analysis for these formations. For example, standard air permeability techniques are often still used on tight gas sands even though the result may be 1 to 2 orders of magnitude higher than in situ permeability. However, with the transient or "pulse decay" technique and computer control it is now possible to perform rapid and accurate permeability measurements on "tight" samples with elevated pore pressure, confining pressure and partial water saturation. This new technology greatly increases the value of laboratory core data by simulating in situ conditions and reducing measurement time.

The experimental results presented in this paper are an extension of some previous work on the effect of partial saturation on gas permeability.[2] Five samples from the Spirit River formation of Alberta, Canada were studied to determine their sensitivity to various brine solutions. The samples were adjacent 4 cm long by 5.08 cm diameter pieces cut vertically from a 20 cm

(7.9 in.) long whole core. This core was from a depth of 1998 m (6556 ft). Gas permeability was measured at in situ pressure on each of the smaller samples as a function of partial saturation using a different fluid in each one. The saturants were distilled water, 1% KCl brine, 5% KCl brine, 5% NaCl brine and 10% NaCl brine.

EXPERIMENTAL TECHNIQUE

The principles and theory of transient permeability measurement methods have been discussed in detail in some previous literature.[3] Basically, the technique employs a jacketed sample in a pressure vessel with a pore pressure line to both ends of the core (Figure 5.1). These lines lead to external reservoirs 1 and 2 with the volume of 1 being much larger than the sample's pore volume or reservoir 2. Initially, pressure in both reservoirs and in the pore space of the sample is equal with valves 1 and 2 open. After closing valves 1 and 2, the pressure in reservoir 1 is changed by a small amount ($\approx$ 1 bar) and after a short wait for thermal equilibrium, valve 1 is opened, thereby creating a pressure gradient across the sample. The differential pressure transducer senses this pressure "pulse" and, as the pulse decays with time, it is recorded so that permeability can be calculated from the rate of decay. An analytical solution to the diffusion problem has been found and is given in Bourbie and Walls.[4]

In practice, the system is much more complex than indicated by Figure 5.1. Because we have five samples in the same vessel and measurements are made on all of them at once, a system as shown schematically in Figure 5.2 is required. A photo of the system is shown in Figure 5.3. Because of the large number of valves and transducers to be actuated or monitored, a small computer and controller are employed. The computer controls the entire measurement procedure including pressure adjustments, decay monitoring, data analysis, plotting and recording. Such automation leaves the operator free to prepare samples, measure porosities, establish saturations, etc. The computer also reduces the possibility of human error which makes the system fast, efficient and safe to operate.

With this system, permeability can be measured from 10^{-8} m^2 (10 nanodarcy) to 10^{-3} m^2 (1 millidarcy) with about 5% accuracy. Confining pressure up to 100 MPa (15,000 psi) and pore pressure to 70 MPA (10,000 psi) are possible along with temperature to about 150°C. The sample can be partially saturated with brine or oil while gas permeability measurements are being performed.

SAMPLE CHARACTERIZATION

The five samples studied all came from a very homogenous 20 cm long section of whole core. It was taken from a depth of 1998 M (6556 ft.) in the Spirit River formation of Western Alberta, Canada. A 5.08 cm diameter core was cut vertically from the whole core and sliced into five pieces each about 4 cm long. Because the five samples came from one piece of whole core, their mineralogy was essentially identical. Table 5.1 gives the average mineralogical breakdown for the five samples. The clays were primarily authegenic illite and chlorite in about equal proportion and, in total, made up about 5% by weight of the sample. Even though mineralogy was very similar, porosities and absolute permeability was somewhat variable as shown in Table 5.2. The permeability measurements were made with nitrogen at 140 bars pore pressure and a hydrostatic confining pressure of 450 bars.

SALINITY AND k_{rw}

To determine the affect of the various brines, each sample was fully saturated with one of the fluids previously mentioned. This was accomplished by placing the sample in a thick walled stainless steel container and evacuating to 10 millitorr for 24 hours. The container was then flooded with de-aerated brine and pressure was increased to 10 MPa (1500 psi). The sample remained under pressure for another 12 hours. After removal from the saturator, the samples were placed on a precise digital balance and dried to a partial saturation of 60%. About 12 hours was allowed for saturation equilibration, after which they were jacketed and mounted inside the pressure vessel. Permeability was measured four times on each sample, then they were removed and brine saturation was reduced to 50% of pore space. This procedure was repeated for each saturation point. Note that only gas is mobil in these experiments. The results of this gas permeability vs. partial brine saturation experiment is shown in Figure 5.4 through 5.8. The data was normalized by plotting the ratio of dry permeability (k_o) to partially saturated permeability for each sample.

DISCUSSION

As can be seen from these plots, gas permeability is affected about equally by each of the saturating solutions tested. Minor differences can be seen in the shape of the curves but considering the differences in absolute permeability and porosity from sample to sample the variations are considered minor. The primary reason for the relative insensitivity to type or amount of dissolved salts is the absence of swelling clays such as montmorillonite. Note also that the dry permeability taken after partial saturation, k_o, is slightly higher than the initial dry permeability from Table 5.2.

After the samples were removed from the pressure vessel, a small piece was removed from each one and gold coated for examination with the scanning electron microscope (SEM). Photos of the clay structure (Figures 5.9 through 5.13) show no detectable change from a sample examined before permeability measurement. These results differ from those of Sampath[5] for samples from the Uinta Basin of Utah. Using similar techniques, Sampath found a marked change in clay morphology after saturation with 2% NaCl and 2% KCl. The Uinta samples contained primarily kaolinite and illite. The different sensitivity of clay to brine in the Spirit River vs. the Uinta Basin samples suggests that care should be exercised in transferring techniques and procedures from one reservoir to another.

CONCLUSIONS

Extensive developmental work has resulted in an automated, multi-sample gas permeameter for tight sands and other low permeability material. The system can accomodate samples from plug size to about 4 inches in diameter with pore pressure, confining pressure and partial water saturation.

The results of tests on five Spirit River sandstones indicate that distilled water, NaCl brine and KCl brine have about equal effect on gas permeability. SEM photos show no change in clay morphology after saturation with water or brine and dry permeability is the same or higher after the partially saturated samples are redried.

NOMENCLATURE

k = gas permeability of sample at a given saturation.

k_o = gas permeability of dry sample.

REFERENCES

1 Gas Research Institute: "GRI Program Plan For Tight Gas Reservoirs", Gas Research Institute, Chicago, Illinois, May 1982.

2 Walls, J.D., "Tight Gas Sand: Permeability, Pore Structure, and Clay", presented at the SPE/DOE Low Permeability Symposium, Denver, May 1981.

3 Walls, J.D., A.M. Nur and T. Bourbie: "Effects of Pressure and Partial Water Saturation on Gas Permeability: Experimental Results", J. Pet. Tech., April 1982.

4 Bourbie, T., and J.D. Walls: "Pulse Decay Permeability: Analytical Solution and Experimental Test", Soc. Pet. Eng. J., October 1982.

5 Sampath, K., and C.W. Keighin: "Factors Affecting Gas Slippage in Tight Sandstones", presented at the SPE/DOE Low Permeability Symposium, Denver, May 1981.

TABLE 5.1 AVERAGE SAMPLE MINERALOGY FROM THIN SECTION

Porosity	7.4 (%)
Quartz	48.8
Chert	13.3
Argillaceous Grains	1.9
Dolomite	9.5
Siderite	3.8
Quartz Overgrowth	14.3
Clay	2.9

TABLE 5.2 POROSITY AND PERMEABILITY OF SAMPLES BEFORE SATURATION

Sample	Porosity (%)	Initial Dry Permeability (μD)	Saturant
6556A	6.8	2.15	Distilled Water
6556B	7.7	5.13	1% KCl
6556C	7.2	2.82	5% KCl
6556D	7.5	5.27	10% NaCl
6556E	7.0	4.54	5% NaCl

FIGURE 5.1 Basic Pulse Decay System

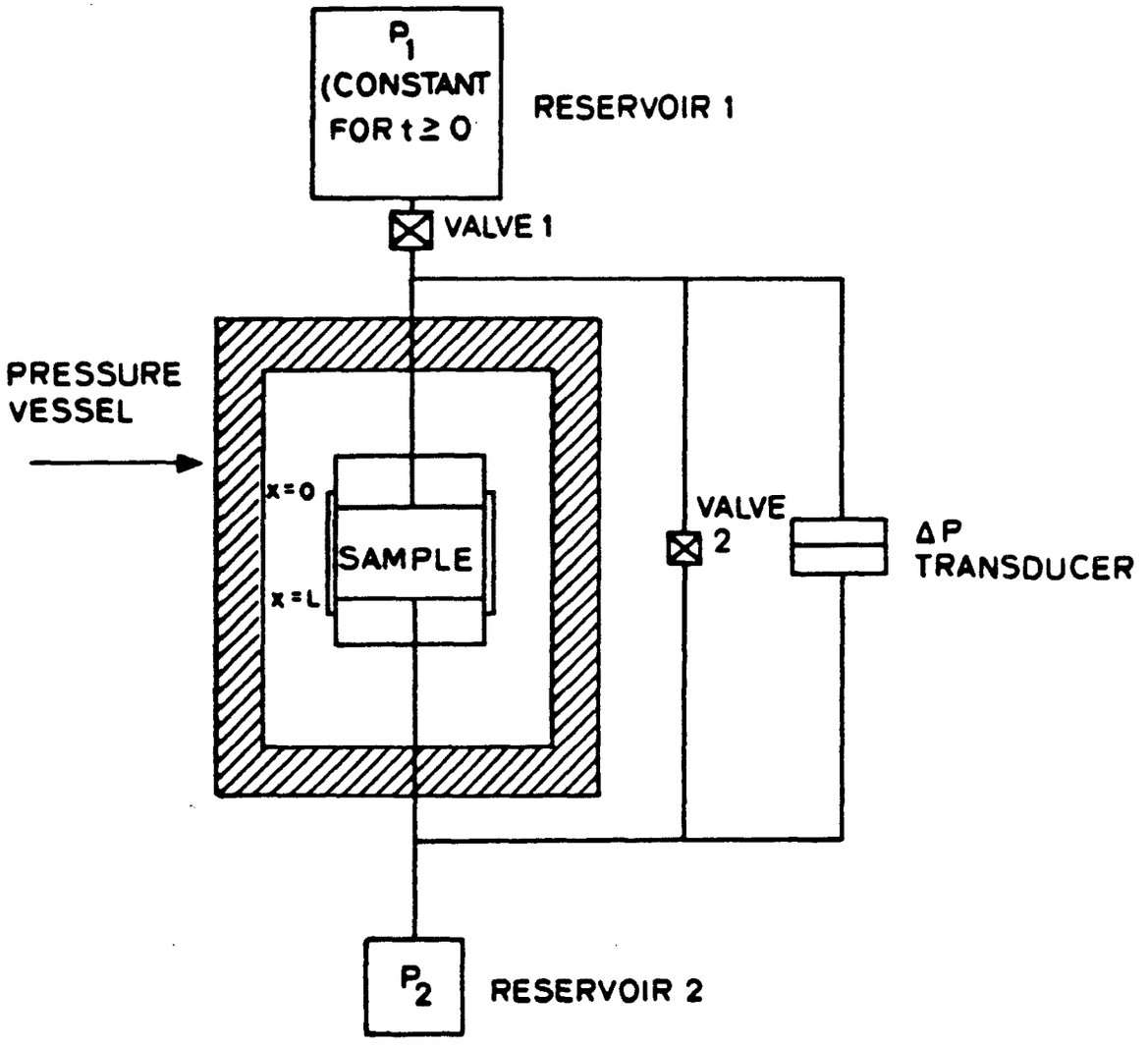

FIGURE 5.2 Multi Sample Automated System

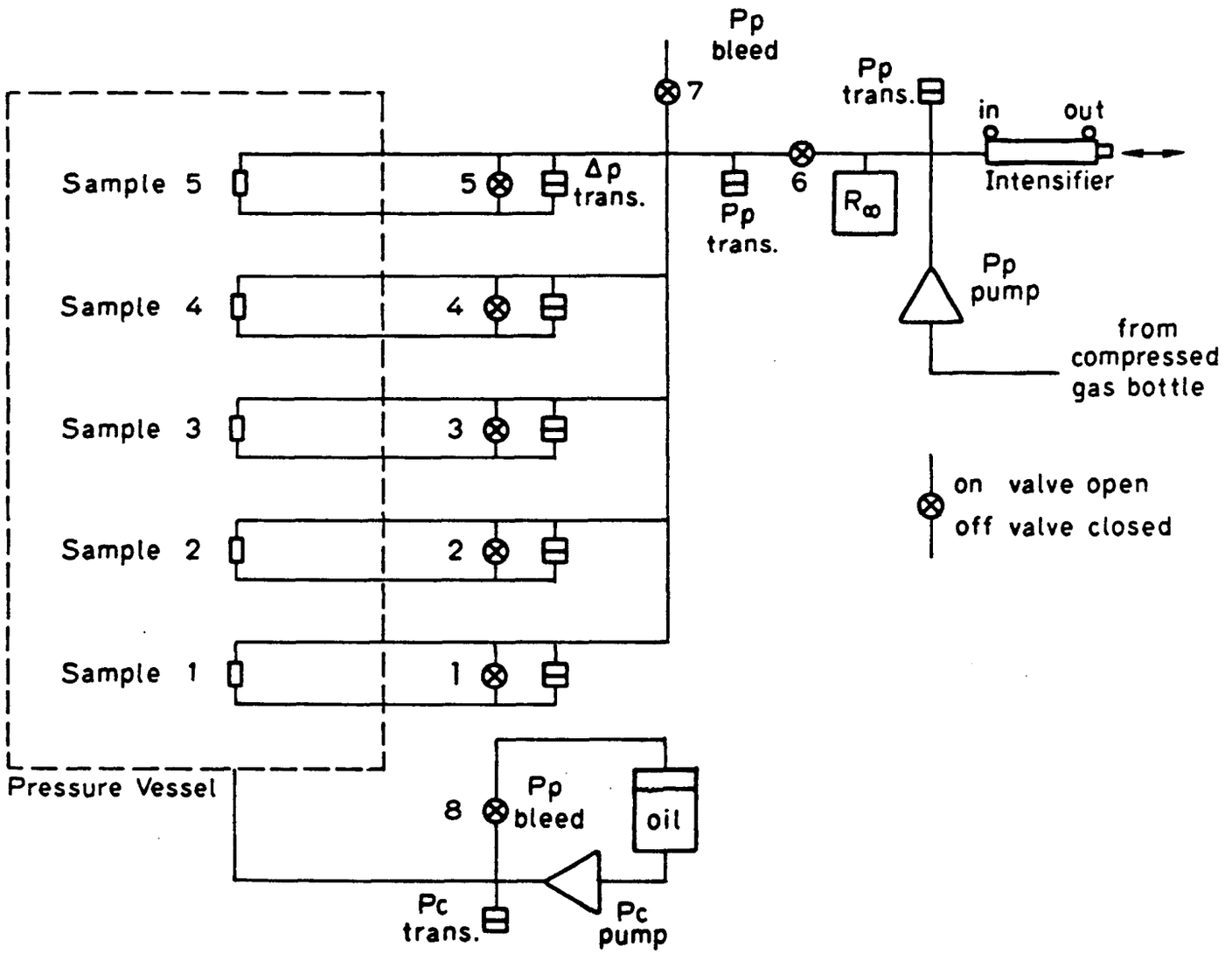

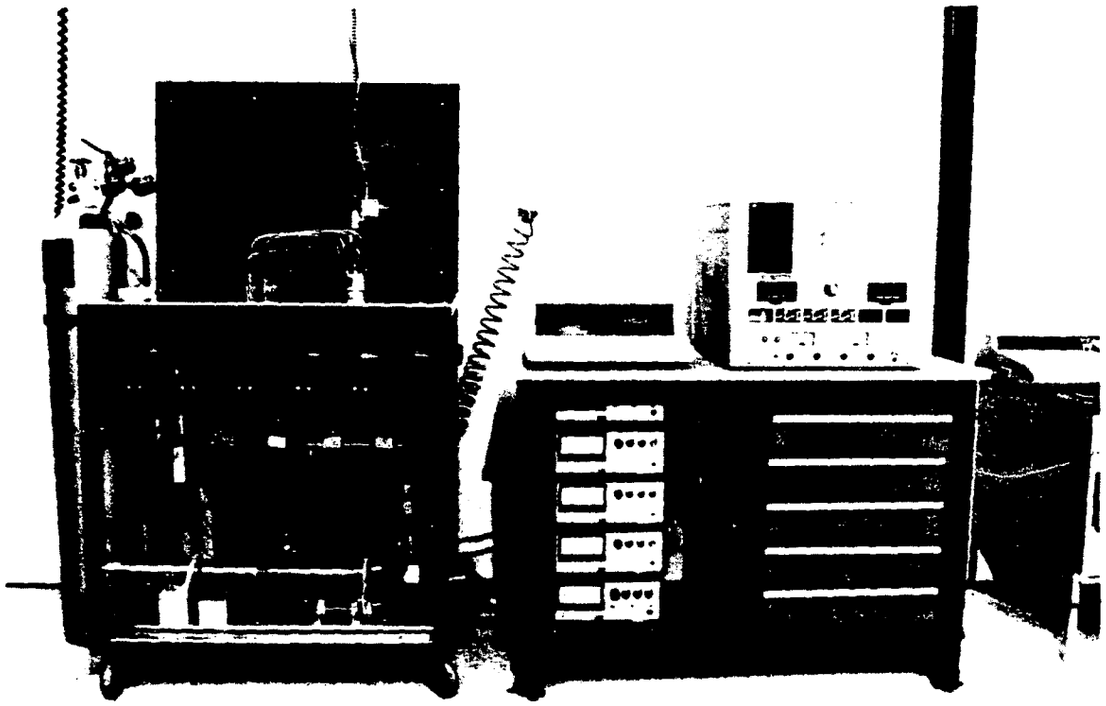

Figure 5.3 Photograph of experimental system.

FIGURE 5.4 Distilled Water

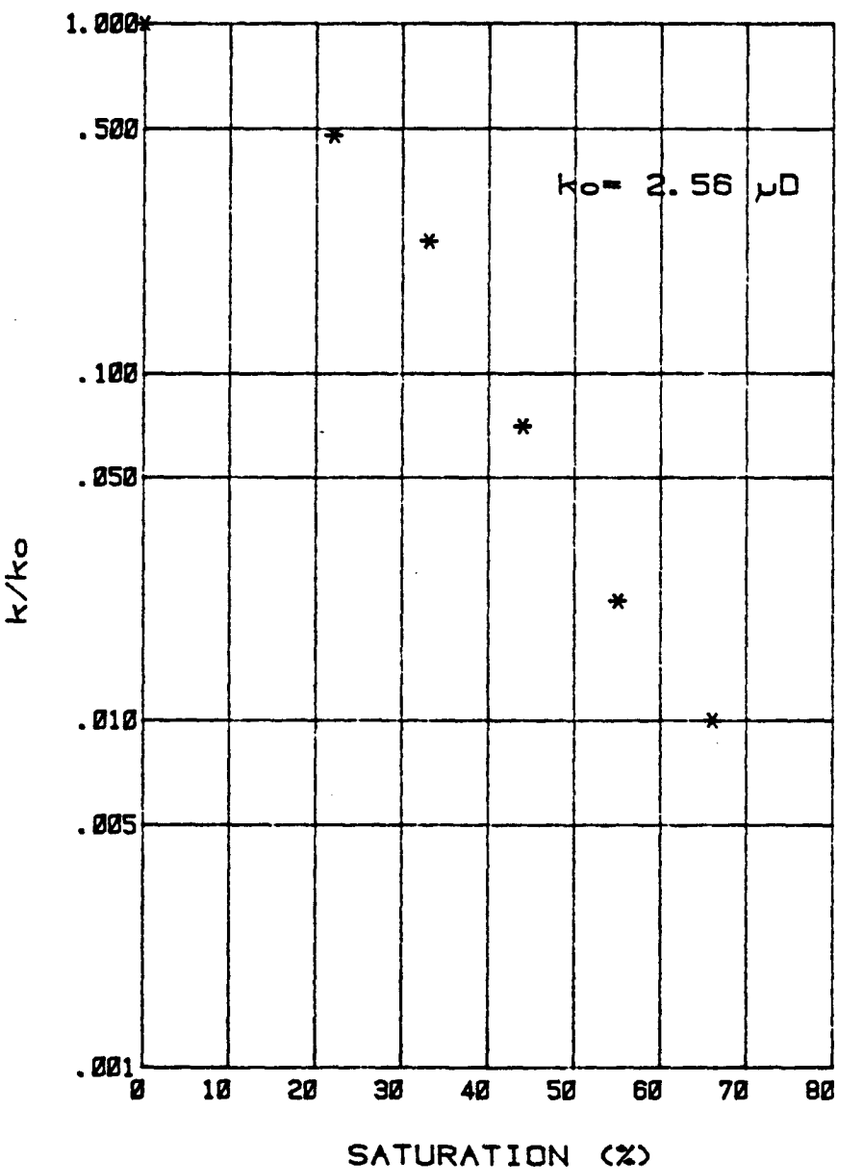

FIGURE 5.5 1% KCl

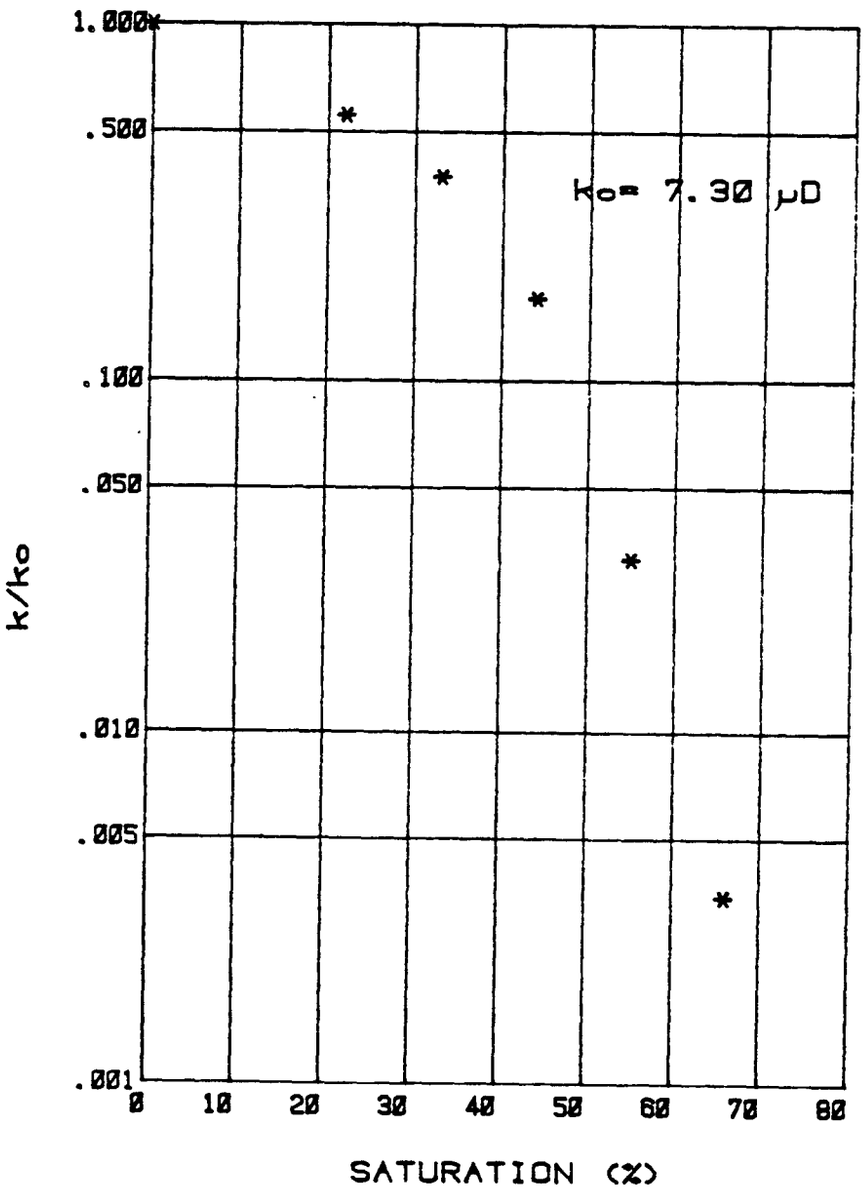

FIGURE 5.6 5% KCl

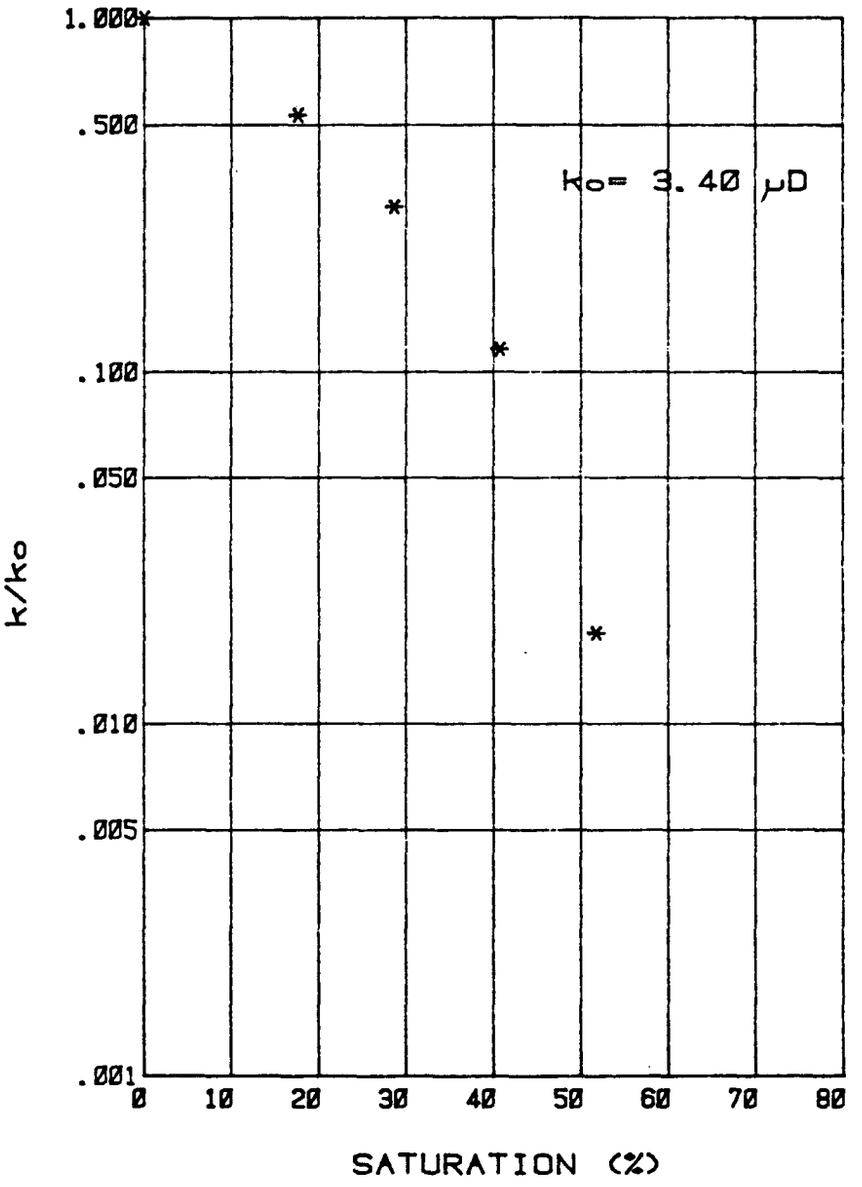

FIGURE 5.7 10% NaCl

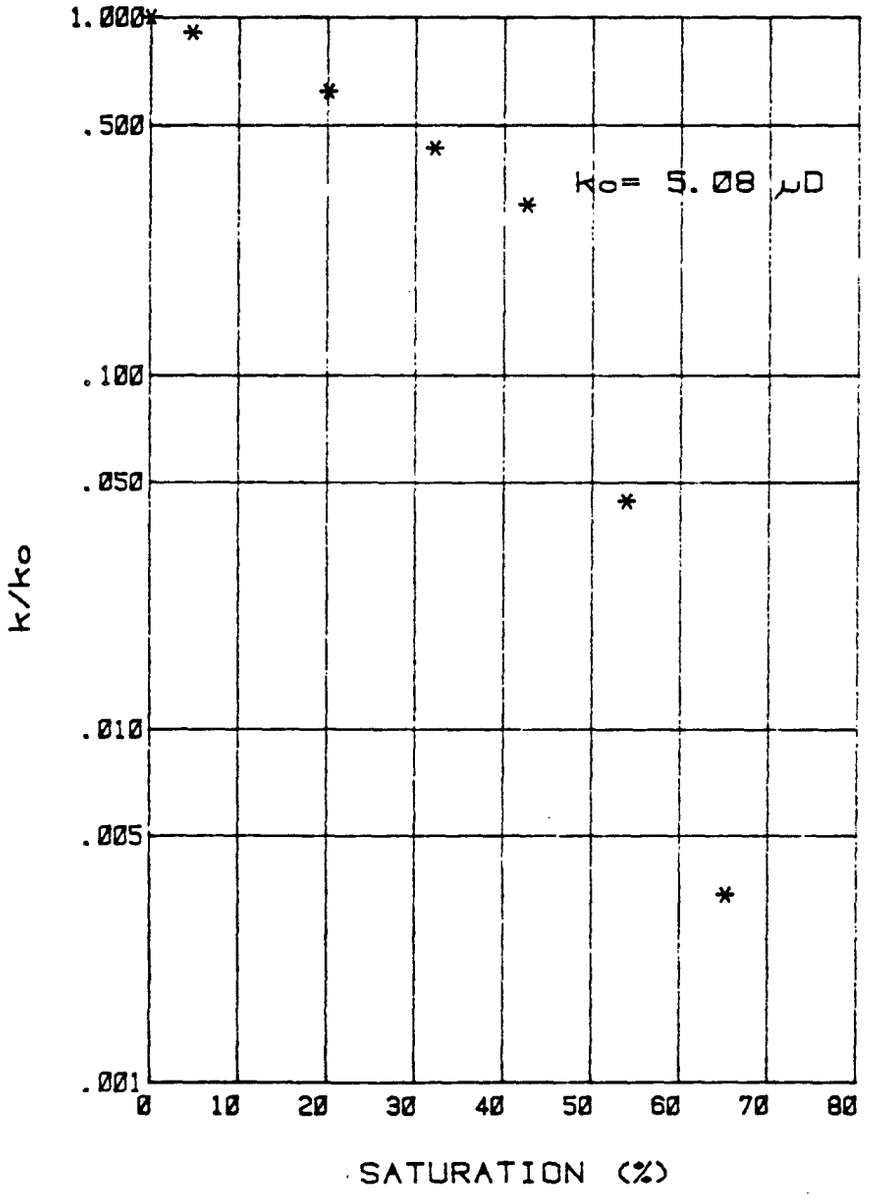

FIGURE 5.8 5% NaCl

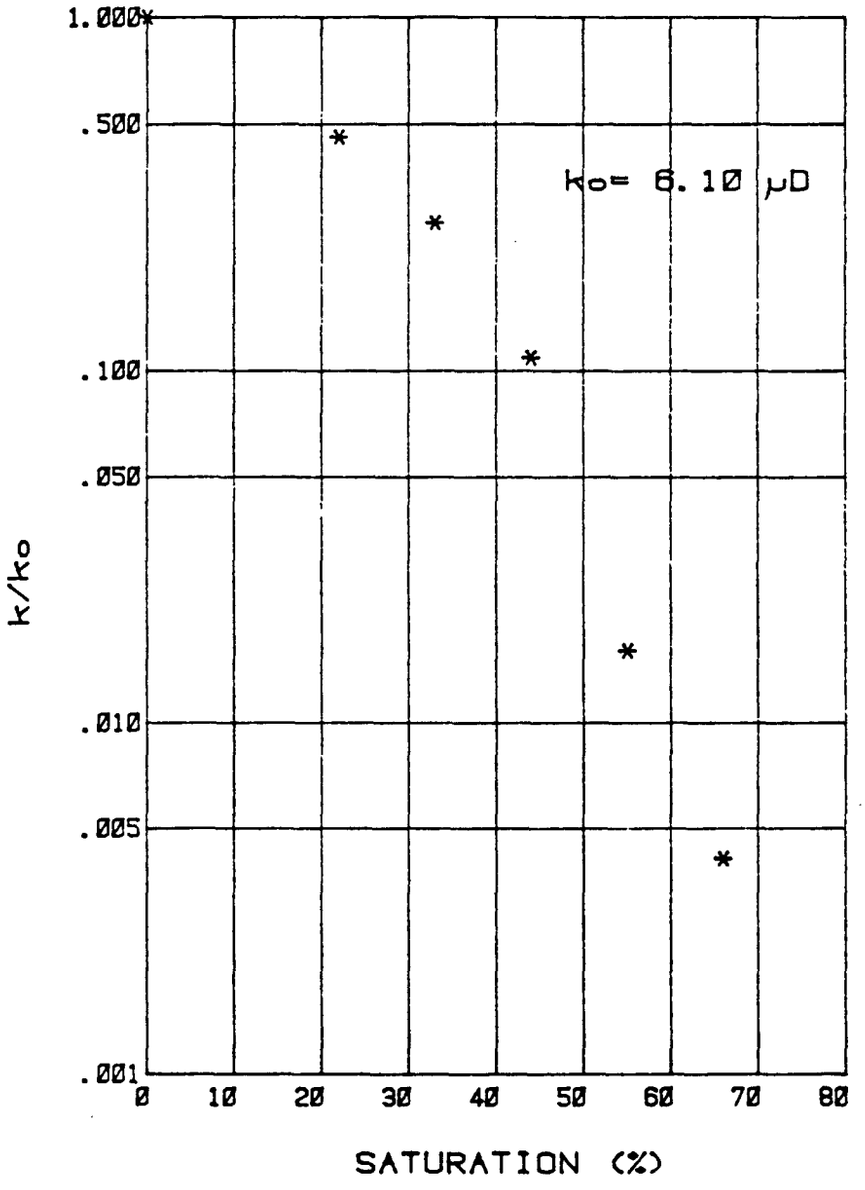

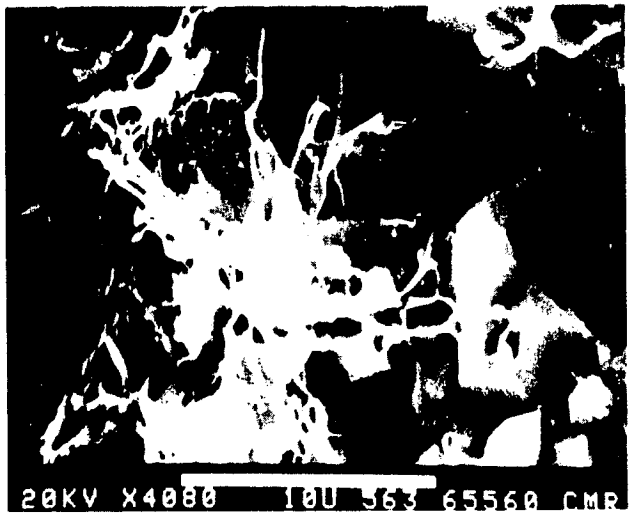

Fig. 5.9 Sample 6556A after permeability vs. saturation measurement

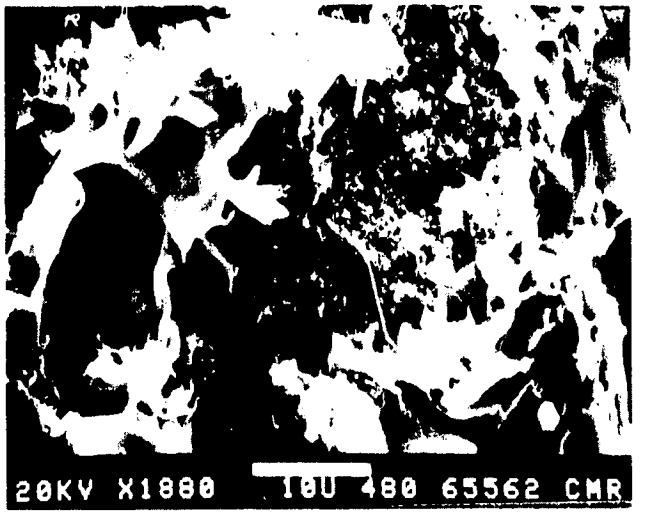

Fig. 5.10 Sample 6556B after permeability vs. saturation measurement

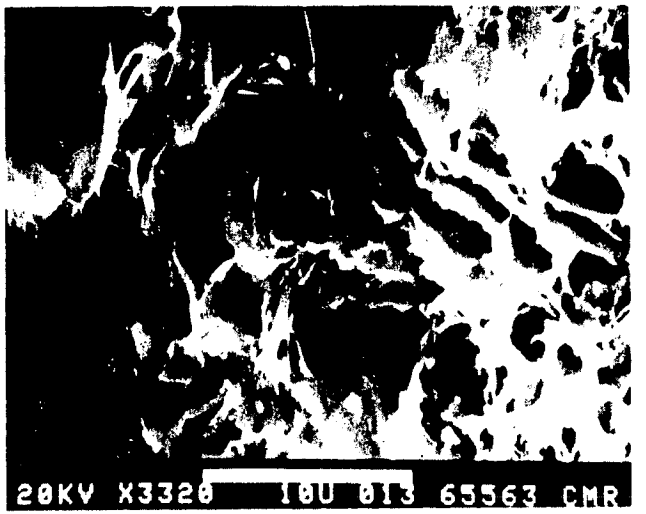

Fig. 5.11 Sample 6556C after permeability vs. saturation measurement.

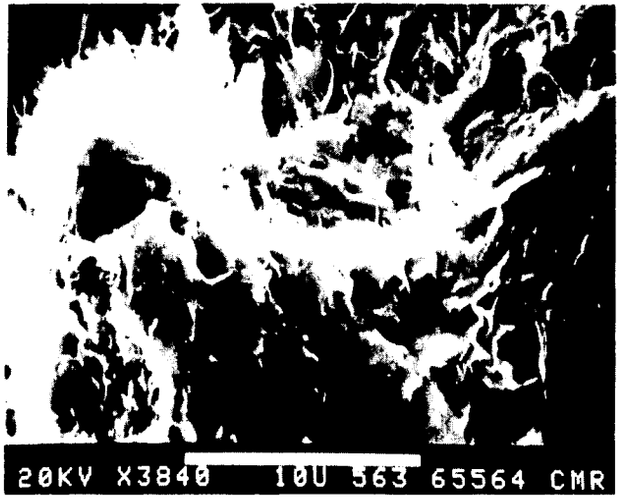

Fig. 5.12 Sample 6556D after permeability vs. saturation measurement.

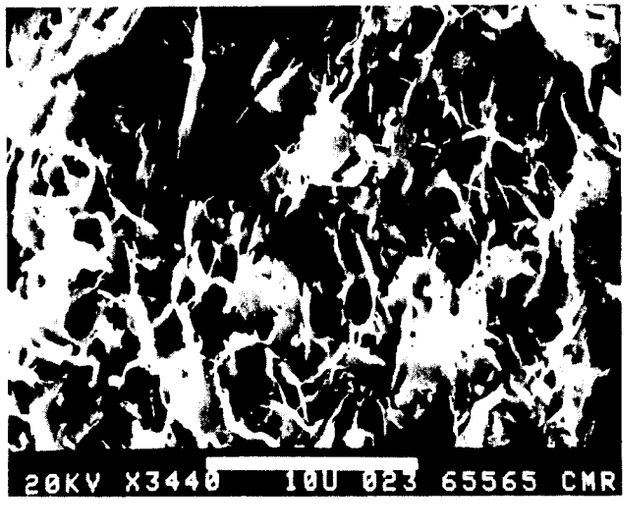

Fig. 5.13 Sample 6556E after permeability vs. saturation measurement.